DALHOUSIE UNIVERSITY

TRACE ELEMENT GEOCHEMISTRY OF BIOTITE FROM THE SCRAG LAKE AND NEW ROSS PLUTONS OF THE SOUTH MOUNTAIN BATHOLITH, NOVA SCOTIA, CANADA: IMPLICATIONS FOR MAGMA DIFFERENTIATION

Kathleen Clark

SUBMITTED IN PARTIAL FULFILLMENT OF THE REQUIREMENTS FOR
THE DEGREE OF BACHELOR OF SCIENCES, HONOURS
DEPARTMENT OF EARTH SCIENCES
DALHOUSIE UNIVERSITY, HALIFAX, NOVA SCOTIA

April 2022

Table of Contents

List of Figures

List of Tables

Abstract

The South Mountain Batholith (SMB) is a 7300 km^2, peraluminous, felsic intrusion occurring in SW Nova Scotia. The batholith consists of 13 plutons emplaced in two different phases between ~385 (Phase 1) and ~368 Ma (Phase 2). Previous research revealed that samples from Phase 2 plutons show significant incompatible trace element variability in biotite compared to Phase 1 plutons. Since Phase 2 plutons tend to be more geochemically evolved, it is not clear if this difference arises due to sampling bias or is an intrinsic property of the second stage of batholith emplacement. Therefore, the goal of this work is to better characterize biotite compositions across a broad compositional range of representative Phase 1 and Phase 2 plutons. Here I present the results of analyses of samples from the Phase 1 Scrag Lake pluton (SGP) and the Phase 2 New Ross pluton (NRP). An electron microprobe and laser ablation ICP-MS have been used to collect major and trace element spot analyses and compositional maps on biotite from a suite of 5 samples from each pluton covering a compositional range of ~68 to ~75 wt% SiO_2. Data for 34 trace elements were obtained, and 18 of these trace elements were used to create trace element maps of 10 different biotite grains. Incompatible trace elements show increases from core to rim within these biotites. For similarly-sized grains and similar whole-rock wt% SiO_2, Phase 1 samples show within grain variation from 10s – 100s μg/g, while variation within phase 2 biotites is 10s – 1000s μg/g. This indicates that the more extreme extent of incompatible trace element variation is an intrinsic property of Phase 2 plutons. Compatible trace elements show opposite trends, with decreases from core to rim. Phase 1 samples show higher concentrations of compatible trace elements, up to 1000 times more than in Phase 2 samples. Some less evolved SGP samples also show oscillatory zoning in Ba and Ga, suggesting that the crystallization and melting of K-feldspar affected these trace element concentrations. Comparing data to simple fractional crystallization models shows that there are trends in the more evolved samples that cannot be explained by fractional crystallization alone, suggesting a non-magmatic process such as hydrothermal activity affected Phase 2 samples. The modeling also shows that Phase 2 biotites have crystallized from more evolved melts than Phase 1 biotites, which explains why there is a difference in the trace element concentrations in biotite between the two phases.

Key Words: South Mountain Batholith, Biotite, Trace Elements, LA ICP-MS Mapping, Magma Differentiation

List of Common Abbreviations

BSE – Back Scatter Electron

EMP – Electron Microprobe

EMPA – Electron Microprobe Analysis

LA ICP-MS – Laser Ablation Inductively Couple Plasma Mass Spectrometer

NRP – New Ross Pluton

SGP – Scrag Lake Pluton

SMB – South Mountain Batholith

wt % - Weight Percent

Acknowledgements

To start, I'd like to thank my supervisor James Brenan for guiding me through this huge project. It was a lot of work, and your guidance was invaluable throughout, I certainly learned a lot in the process. I would also like to extend this thanks to everyone else in the Brenan research group; you've all helped out and offered guidance at one point or another and I am eternally grateful. I also gratefully acknowledge support from the Nova Scotia Department of Natural Resources and Renewables Mineral Resources Development Fund for this project. I would also like to give an extended thank you to those in the department of Earth and Environmental Sciences as well; I've gotten help, inspiration, and/or encouragement from so many of you along the way. Finally, I'd like to thank my family and friends for supporting me along the way, especially my sister Danielle, who's knowledge of photo editing was invaluable in making Figures 9, 10, 11, 12, 17, 18, and 19.

1.0 Introduction

1.1 Previous Research and Motivation for Study

The South Mountain Batholith (SMB), Nova Scotia, is a large, multiphase, granitic intrusion noted for showing remarkable geochemical homogeneity across its two phases of formation (Macdonald et al., 1992). However, more recent research by Brenan et al. (in preparation), has shown significant trace element geochemical variability within the biotites of the SMB. As Figure 1 shows, an incompatible trace element such as Ta can exhibit variation of several orders of magnitudes higher in samples from the later Stage 2 plutons compared to earlier Stage 1 pluton samples.

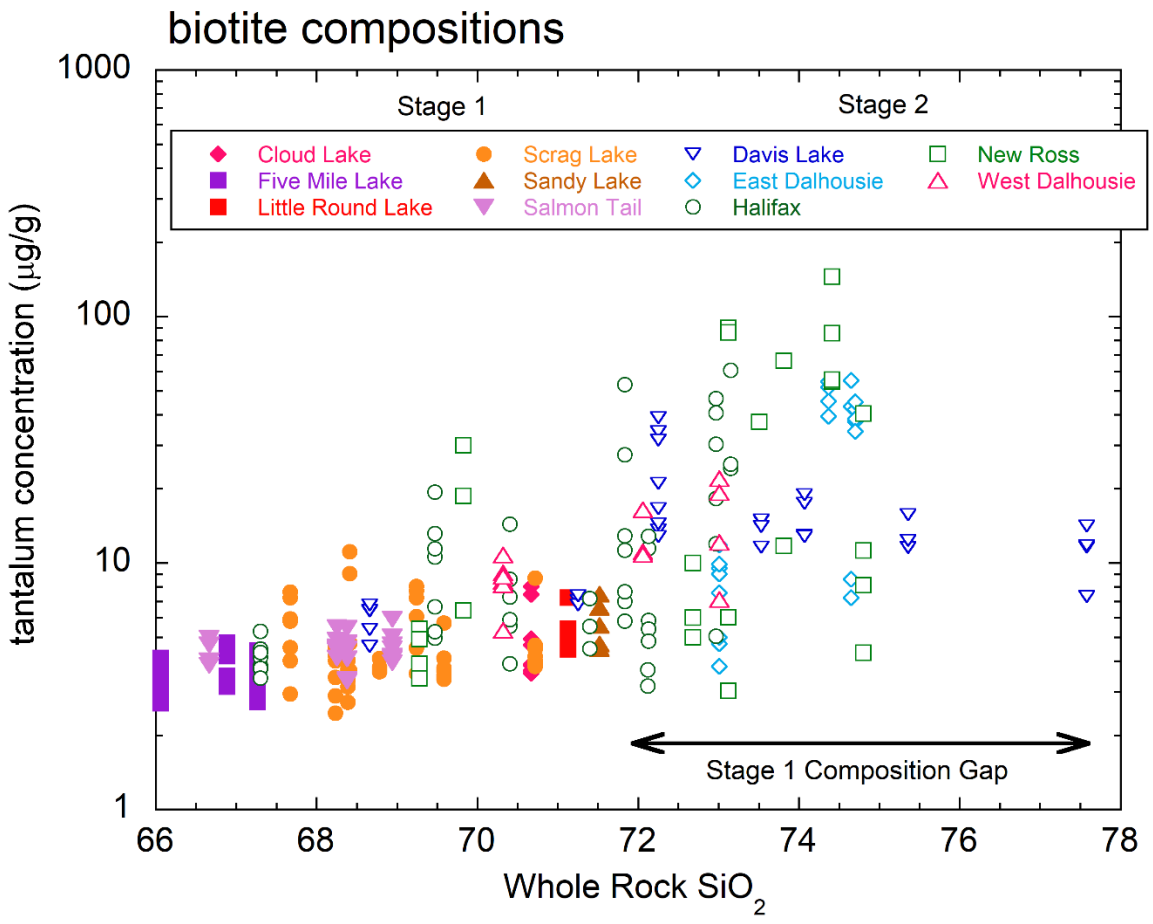

Figure 1 – Variation in the Ta concentrations in biotites vs. the whole rock SiO_2 wt % for samples from every pluton of the SMB. It can be seen that most Stage 1 samples range from 1-10 µg/g Ta, while Stage 2 samples can vary from 1 – 110 µg/g Ta. Highlighted to the right of the graph is the Stage 1 "Composition Gap", where data from Stage 1 samples is lacking.

However, it is not known if this difference in trace element variation is an inherent feature of Stage 2 of the SMB, or if instead due to a sampling bias. The Stage 1 "Composition Gap" (Figure 1), is defined as the range in whole rock SiO_2 concentrations for which data representing both intrusive phases are lacking. In this case, there is a lack of data for the more SiO_2-rich, or chemically evolved, Stage 1 plutons. As such, the main goal of this research is to fill this gap to determine to what degree there is trace element geochemical variability in Stage 1 biotites in the SMB.

Biotite is a sheet silicate mineral with the general chemical formula $K(Fe,Mg)_3AlSi_3O_{10}(OH)_2$, and it is common throughout both intrusive phases of the SMB. The crystal structure of biotite allows it to host a wide variety of elements of differing size, charge, and geochemical affinity. Several of these elements preserve information about the host magma, such as the oxygen fugacity, volatile content, and temperature (Azadbakht and Lentz, 2020; Henry et al., 2005; Mohammadi et al., 2021). The importance of understanding the origin of the differences in the extent of trace element variation in biotite, especially the relative enrichment of Ta (and some other granophile ore metals) in Stage 2 samples, is that it informs on the element enrichment processes during magma evolution which could lead to ore formation in the SMB.

1.2 Approach and Objectives

This research was done by comparing samples from a representative Stage 1 pluton (Scrag Lake) to samples from a representative Stage 2 pluton (New Ross), with a focus on gathering data from samples with a wide range of whole rock SiO_2 concentrations. Whole rock SiO_2 is a metric for the extent of igneous differentiation a sample has experienced; the higher the SiO_2 concentration the more differentiated the sample. These comparisons were done using electron microprobe analysis to produce major element data for a suite of samples, and laser ablation inductively coupled plasma-mass spectrometer (ICP-MS) analysis was done to produce trace element maps for select biotite grains.

In addition to the goal of using this data to determine the extent of trace element variability in Stage 1 of the SMB, other objectives were achieved, including an interpretation of the origin of the trace element variability and any implications for the evolution of the SMB. The initial hypothesis was that there should be some incompatible trace element variability in more evolved Stage 1 samples, but not to the same degree as Stage 2 samples. This initial hypothesis was supported by the trace element maps, with Stage 2 samples showing higher concentrations and greater core to rim variations in incompatible trace elements compared to Stage 1 samples.

2.0 Geological Setting and Geochemistry of the South Mountain Batholith

The South Mountain Batholith is located in the Meguma Terrane in southwestern Nova Scotia (Figure 2). This terrane represents the most eastward terrane of the Appalachian orogenic belt and is comprised of the Cambro-Ordovician Meguma supergroup, and the Siluro-Devonian White Rock and Torbrook Formations (Macdonald, 2001; Shellnutt and Dostal 2012). The Meguma supergroup is comprised of psammites of the Goldenville Formation overlain by the pelites of the Halifax Formation, while the White Rock and Torbrook Formations are mixed volcanic, volcanoclastic, and metasedimentary rocks (Macdonald, 2001).

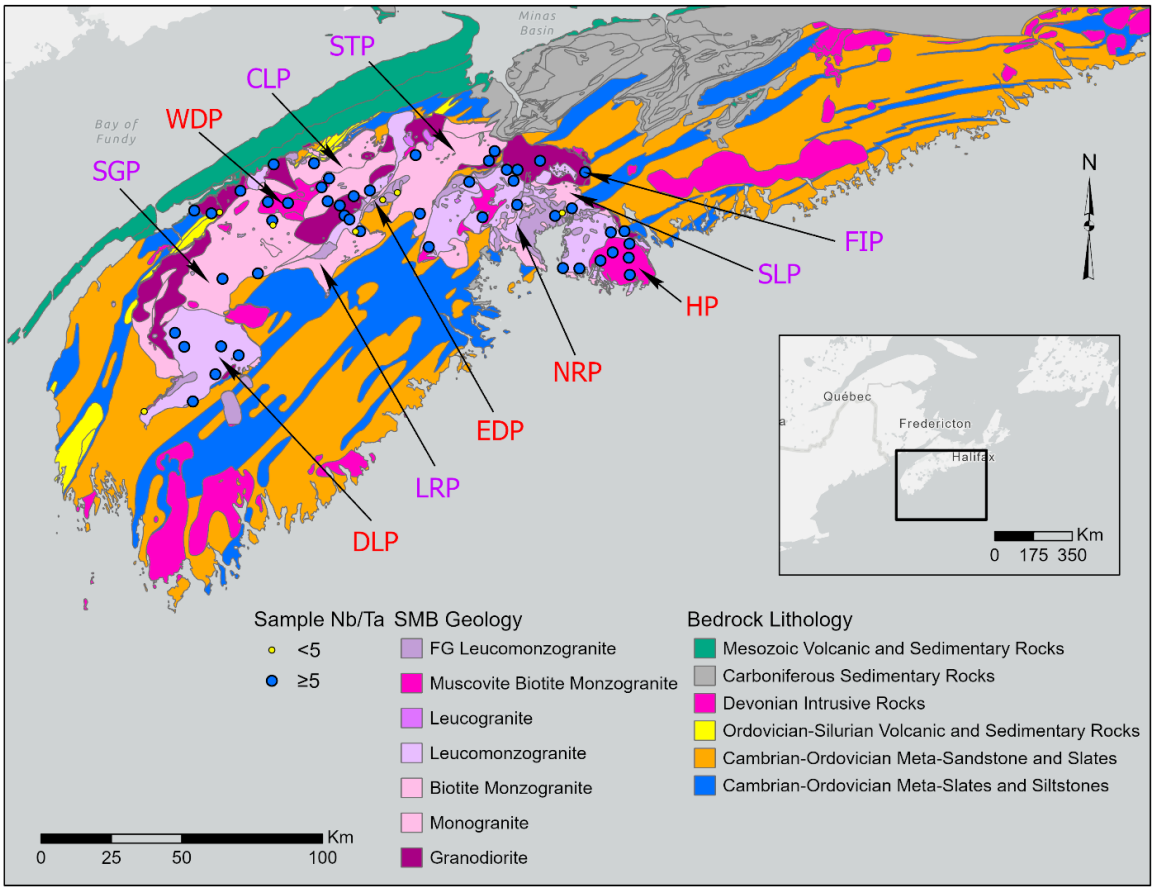

Figure 2 – Map showing the location of the SMB and its plutons, with respect to the surrounding lithology of southwestern Nova Scotia, Canada. Stage 1 plutons are labeled with purple text while the Stage 2 plutons are labeled with red text. Pluton abbreviations and stages are as follows: Davis Lake Pluton (DLP; 2); Little Round Lake Pluton (LRP; 1); East Dalhousie Pluton (EDP; 2); New Ross Pluton (NRP; 2); Halifax Pluton (HP; 2); Sandy Lake Pluton (SLP; 1); Five Mile Lake Pluton (FIP; 1); Salmon Tail Pluton (STP; 1); Cloud Lake Pluton (CLP; 1); West Dalhousie Pluton (WDP; 2); Scrag Lake Pluton (SGP; 1). (Brenan et al., in preparation).

These rocks underwent regional metamorphism and deformation in the mid to late Devonian due to the Acadian orogeny, and during this timeframe several granitic intrusions, including the South Mountain Batholith, were emplaced (Macdonald, 2001). These intrusions are divided into “Central” and “Peripheral” groups based on their mineralogy and geochemistry (Tate and Clarke, 1997). The “Central” intrusions are peraluminous granodiorites to leucogranites, and include the South Mountain Batholith, the Musquadoboit Batholith, and granitoids in the New Liscomb Complex (Tate and Clarke, 1997). The “Peripheral” intrusions are metaluminous to peraluminous, and range from tonalites to leucogranites with some containing hornblende (Tate and Clarke, 1997). The “Peripheral” group includes the Port Mouton, Shelburne, and Barrington Passage plutons (Tate and Clarke, 1997).

The South Mountain Batholith is the largest of these intrusive bodies, exposed over an area of ~7300 km^2 of southwestern Nova Scotia (Shellnutt and Dostal, 2015). The batholith is comprised of 11 plutons, which are further divided into Stage 1 and Stage 2 intrusive phases (see Figure 2). There are six main rock types represented by samples from the South Mountain Batholith: biotite granodiorite, biotite monzogranite, muscovite-biotite monzogranite, coarse-grained leucomonzogranite, fine-grained leucomonzogranite and leucogranite (MacDonald et al., 1992). The earlier Stage 1 plutons are comprised mainly of granodiorites and monzogranites, which intruded around 381 Ma and are considered the less evolved parts of the South Mountain Batholith (Bickerton et al., 2019; Shellnutt and Dostal, 2012). The later Stage 2 plutons are comprised mainly of more evolved leucomonzogranites and leucogranites that intruded later, around 376 – 368 Ma (Bickerton et al., 2019; Shellnutt and Dostal, 2012). The main mineralogy of the South Mountain Batholith is quartz, K-feldspar, and plagioclase, with lesser amounts of biotite, muscovite, aluminosilicates (sillimanite or andalusite), cordierite, garnet, and tourmaline. Common accessory minerals include ilmenite, apatite, zircon, monazite, and rutile (Brenan et al., in preparation).

The South Mountain Batholith is classified as an S-type, peraluminous granitoid, with modelling suggesting it formed by melting of a crustal source, then fractional crystallization and assimilation (Shellnutt and Dostal; 2012, 2015). The whole rock SiO_2 range of the South Mountain Batholith is ~67-74 wt %, and other elements show continuous trends across this range. The concentrations of major element oxides in whole rock analysis, such as TiO_2, FeO, MnO, and CaO, all show a continuous decrease in concentration with increasing SiO_2 (MacDonald et al., 1992), which is illustrated in Figure 3. There are also similar trends in the trace element whole rock concentrations; compatible trace elements (i.e. Ba, Sr, Zr, V, Hf, Sc, and La) decrease and incompatible trace elements (i.e. Rb, Ta, U, Li, F, Sn, and W) increase with increasing SiO_2 wt % (Macdonald et al., 1992). In addition to these trends, samples from both phases show very similar whole rock geochemistry, despite higher proportions of the more evolved compositions in the Stage 2 sample suite.

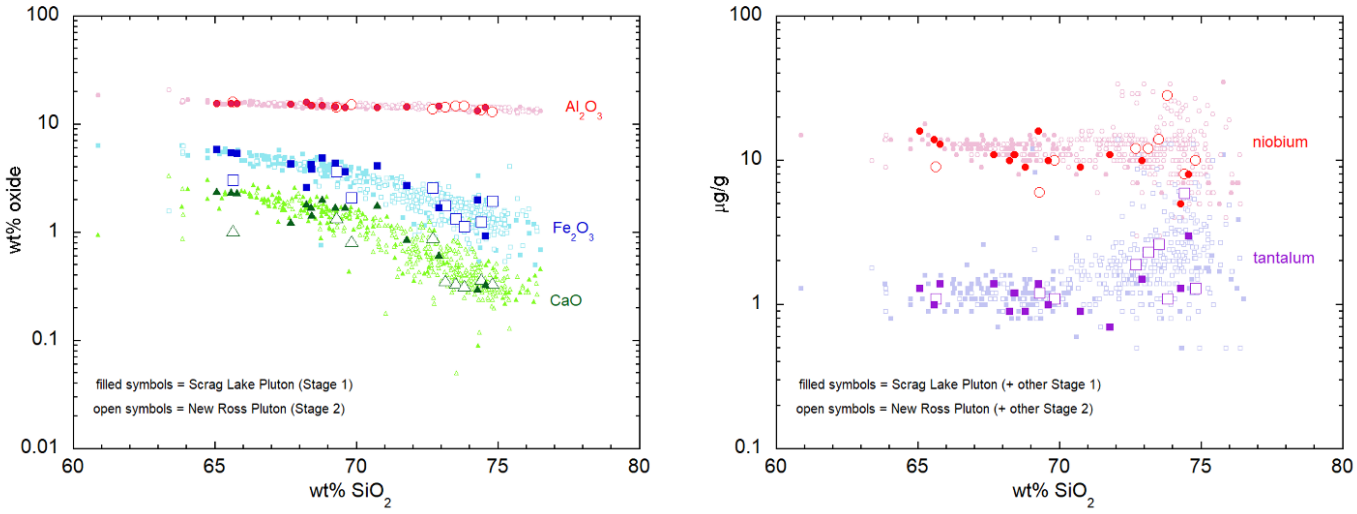

Figure 3 – Plots comparing the whole rock data for several major element oxides (left plot) and trace elements (right plot) against the whole rock SiO_2 wt %. Stage 1 samples are filled symbols and Stage 2 samples have open symbols. The larger data points are from samples used in this study, and the smaller symbols represent data from the rest of the SMB.

For all these similarities, there are some compositional differences between Stage 1 and Stage 2 samples, most notably in the whole rock Li and F content (Figure 4). In the more

evolved samples from both phases there is a divergence in the whole rock Li and F, showing an enrichment in Stage 2 samples and a depletion in Stage 1 samples.

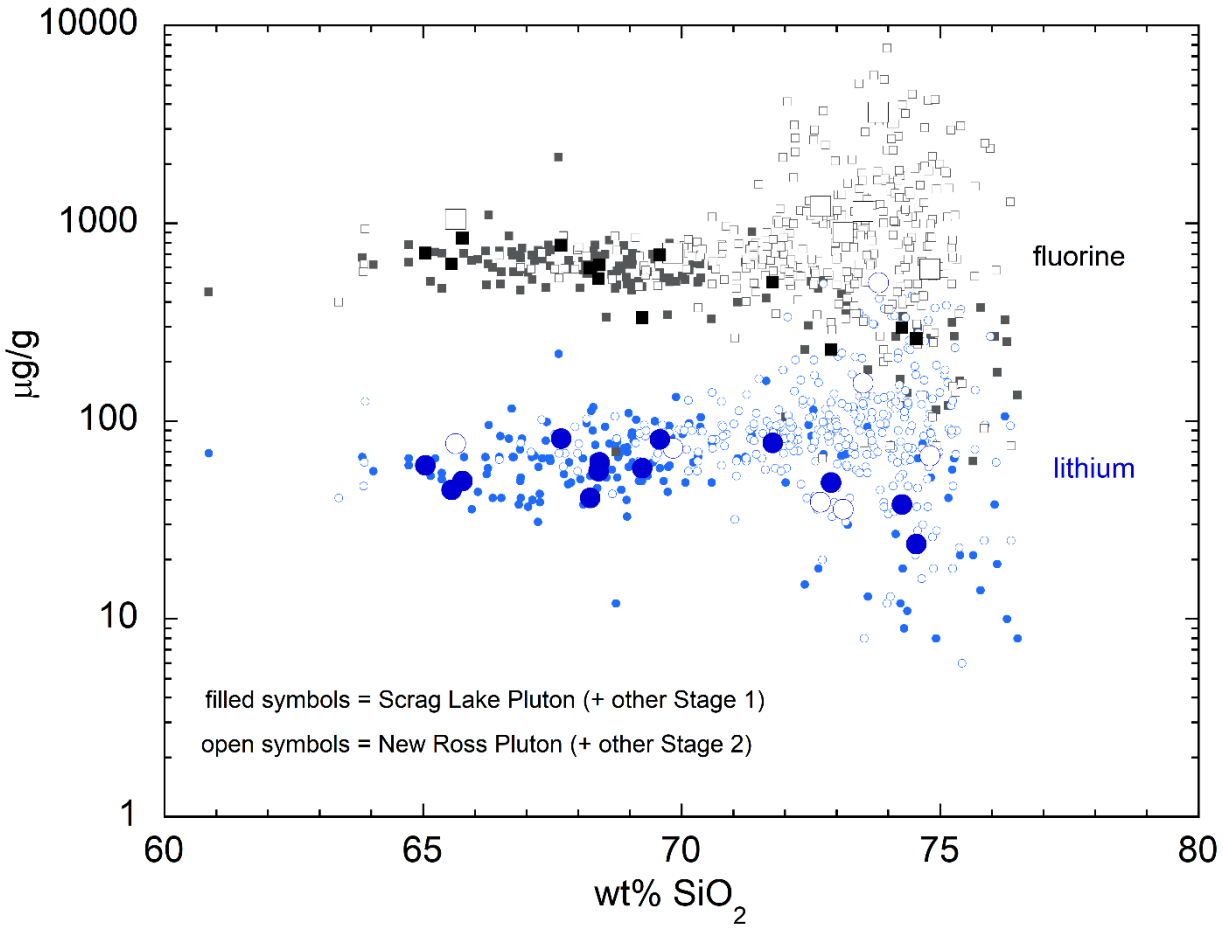

Figure 4 – Li and F whole rock concentrations versus the whole rock SiO_2 wt %. Once again, Stage 1 samples are filled symbols and Stage 2 samples have open symbols. The larger data points are from samples used in this study, while the smaller symbols represent data from the rest of the SMB. It can be seen that the datasets overlap at lower SiO_2 values but there is divergence at higher SiO_2 values, showing the Li and F concentrations increasing in Stage 2 samples and decreasing in Stage 1 samples.

For this study, the representative Stage 1 pluton chosen is the Scrag Lake Pluton (SGP), and the representative Stage 2 pluton chosen is the New Ross Pluton (NRP). The SGP is the largest pluton in the SMB and comprises about a third of the SMB total surface area (Shellnutt & Dostal, 2012). The SGP rocks range from biotite granodiorites to biotite monzogranites, while the NRP is comprised of more felsic rocks from leucomonzogranites and leucogranites (more details on sample petrography can be found in section 4.1 and the Appendix).

3.0 Sampling and Methods

3.1 Sampling

The main goal of this study was to gather trace element geochemical data from biotite from the more evolved compositions of a Stage 1 pluton of the SMB to fill in the Stage 1 "data gap". The Scrag Lake Pluton was selected because of the availability of samples representing a wide compositional range, including those with whole-rock SiO_2 concentrations overlapping with other Stage 2 Pluton samples. The whole-rock SiO_2 concentration is used as an indicator of how evolved a sample is, in terms of the extent of geochemical differentiation, with a higher value indicating a greater level of differentiation. In total, eight SGP samples were chosen, covering a range in SiO_2 concentrations from 65.04 to 74.54 wt %. Although the goal was to gather data from the more SiO_2-rich samples, it was considered important to check samples across the whole compositional range to determine if there is a point at which significant trace element variability begins. For comparative purposes, a suite of five samples was also chosen from the Stage 2 New Ross Pluton, covering a similar range of SiO_2 concentrations from 69.28 to 74.80. In addition to whole-rock SiO_2 concentration, samples were also selected based on their Nb/Ta ratio, which is considered to be an indicator of magmatic vs. non-magmatic processes in felsic igneous rocks (Ballouard et al., 2016; 2020). Most samples have magmatic Nb/Ta > 5, but 2 samples have Nb/Ta < 5, suggestive of a hydrothermal influence.

Samples from the SGP were obtained from the Nova Scotia Core Library and cut into slabs that were made into polished thin sections at Saint Mary's University. The NRP samples were obtained as polished thin sections chosen from a collection previously studied by Brenan et al. (in preparation). Several biotite grains per section were chosen for analysis, based on the size, degree of alteration, and a lack of accessory mineral inclusions. The size of the biotites was an important factor when deciding which grains to use to produce trace element maps; larger biotite grains displayed trace element zoning clearer than smaller grains, but if the grain was too large then it would take too much time to map. Most grains chosen to map had average lengths & widths of 1000 – 2000 microns. A lack of alteration and inclusions was also desirable to prevent interferences with the biotite analysis. Grains were analysed by electron microprobe for major element compositions and laser ablation ICP-MS for trace elements. Trace element

analyses were done as individual spots and a subset of grains were mapped using long raster scans (see below for details).

3.2 Trace element mapping protocol

The procedure for the preparation of trace element maps follows the protocol employed by Azadbakht and Lentz (2020) in their study of trace element variation in biotite from Devonian-aged granites from New Brunswick. To start, samples were characterized using transmitted and reflected light microscopy using a standard petrographic microscope in Dalhousie's Petrology Teaching Laboratory. This was done to identify suitable biotite grains for later analysis, and to create a database of general petrographic descriptions. After this, samples were imaged and analyzed for major elements using the JEOL JXA-8200 Electron Probe Micro-Analyzer (EPMA) at Dalhousie's Robert M. MacKay Electron Microprobe Lab. Biotite analyses were done using an accelerating voltage of 15kV, a beam current of 20 nA, and a 1 µm focused beam to limit sample damage. Standards for biotite analysis were biotite (Fe, Al, Si, K, Mg), pyrolusite (Mn), kaersutite (Ca, Ti), albite (Na), tugtupite (Cl) and apatite (F). Count times were 90 and 40 seconds on peak for F and Cl, respectively, and 20 seconds on peak for all other elements. The spectral interference from the Fe lα1,2 emission line (705 eV) on the F kα line (676.8 eV) was determined by measuring the F ka intensity in Fe-metal, which was then used to calculate an appropriate correction factor. Analysis of natural hematite yielded F concentrations of < 0.02 wt%, confirming the efficacy of this correction method. Grains that were being considered for subsequent trace element mapping were then checked for accessory mineral inclusions, and the final list of grains for further analysis was determined. In addition to spot analyses, major element maps were produced for each biotite grain that was chosen to be mapped using laser ablation ICP-MS.

After textural and major element analysis, the grains were measured for trace elements using laser ablation ICP-MS at Dalhousie's Health and Environments Research Centre (HERC) lab. The laser ablation ICP-MS configuration employs a Nd:YAG laser connected to a Thermo Scientific iCAP Q ICPMS mass spectrometer with helium transporting the ablated aerosol from

the sample chamber to the mass spectrometer. Trace element maps were produced by ablating a grid of adjacent parallel lines long enough to cover the entire biotite grain and include some of the surrounding matrix. A schematic of the scan configuration is shown in Figure 5. Each ablation line was done with a 20 µm diameter beam size, a 10 Hz laser repetition rate, and a 20 µm/s ablation speed. After completing each scan, the laser was blanked and background counts were collected for 20 seconds with helium flushing the cell. The stage was then moved so that the subsequent scan was done adjacent to the previous one. Two measurements were also done on the NIST610 standard reference material, a trace element doped glass, at the start and end of the map acquisition, and after every 40 to 50 scans. The following isotopes were measured during each analytical scan: 7Li, 27Al, 31P, 43Ca, 44Ca, 45Sc, 49Ti, 51V, 52Cr, 55Mn, 57Fe, 59Co, 60Ni, 61Ni, 63Cu, 65Cu, 66Zn, 69Ga, 71Ga, 73Ge, 75As, 85Rb, 88Sr, 89Y, 90Zr, 93Nb, 95Mo, 111Cd, 113In, 115In, 118Sn, 121Sb, 133Cs, 137Ba, 139La, 140Ce, 141Pr, 146Nd, 147Sm, 153Eu, 157Gd, 159Tb, 163Dy, 165Ho, 166Er, 169Tm, 172Yb, 175Lu, 178Hf, 181Ta, 182W, 206Pb, 207Pb, 208Pb, 209Bi, 232Th and 238U.

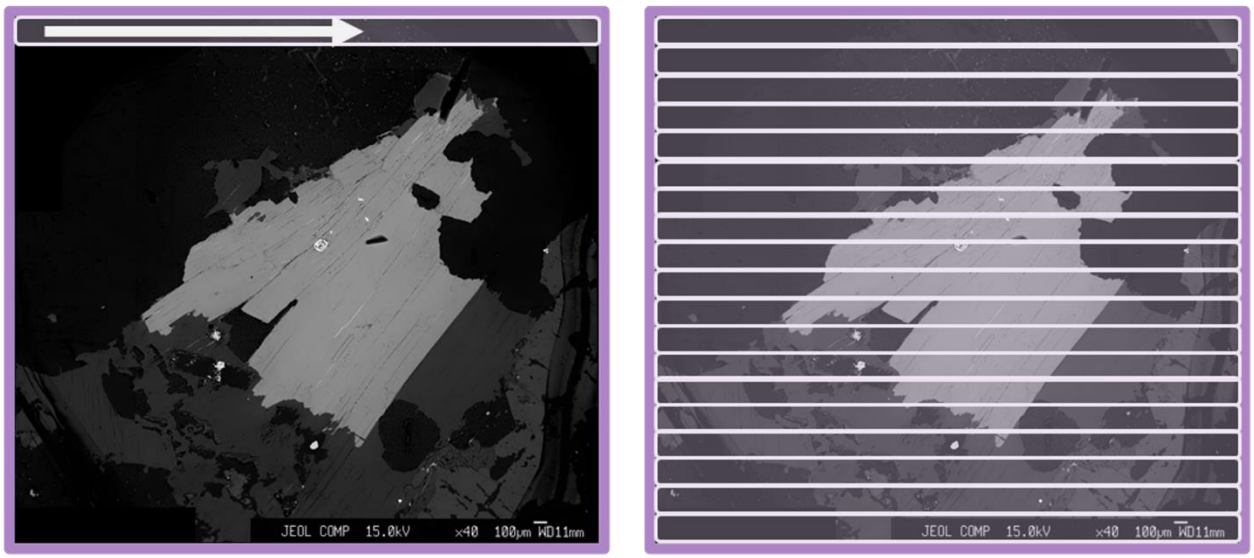

Figure 5 – An outline of the process used to generate laser ablation trace element maps. To start, one line scan moves across the mapping area, in this case left to right (left image). Each scan is evenly spaced so that the entire mapping area is covered by line scans at the end of the process (right image).

3.3 Data Analysis

Raw time-resolved intensity data for each isotope from the analytical scans were processed using the Iolite (v.4) software (Paton et al., 2011). The processing involves selection of background and signal portions, and adjusting the integration interval to avoid intensity spikes either from plasma instability or the presence of inclusion phases. The Ti and Al major element data collected by electron microprobe were used to correct the data for differences in ablation yield between sample and standard. Spot analyses were corrected using the Ti content of each biotite, while the trace element maps were corrected using the biotite Al content. Because the trace element maps include a portion of surrounding phases, the abundances are only quantitative within the biotite grains, owing to differences in ablation yield for other phases. The imaging options tool of the Iolite 4.0 software was used to create the trace element maps and to collect trace element concentrations from these maps (Paton et al., 2011; Petrus et al., 2017).

3.4 Limitations and Delimitations

There are several limitations and delimitations when it came to sample selection and data collection during this project. To start, sample selection was limited based on the existing samples in the Nova Scotia Core Library and at Dalhousie University. As well, while the focus of the project was on more evolved SGP samples, these samples tended to have less useful biotite grains for mapping and analysis as they were usually smaller in size and showed frequent alteration to chlorite. Also, although the larger biotite grains accentuate trace element variations better when it came to mapping, such large grains are rarer in the evolved samples. Larger grains also require more time to map using EMPA and laser ablation ICP-MS, so samples had to be selected considering a reasonable collection time. Some large grains could take more than 10 hours to map, which was not feasible in most cases.

The other main limitation in this project was the availability of analytical time on both the electron microprobe and laser ablation ICP-MS. Both instruments are used by other researchers, and thus data collection time was limited by availability. As well, both instruments

experienced operation problems during the project, which meant waiting for repairs before data collection could continue. As such, the data collection protocol could not always be followed in some cases (i.e., laser ablation spot analysis was done, then EMPA later), which in some cases required additional sample polishing.

4.0 Results

4.1 Summary of textures

The samples from this study range in composition from granodiorite and monzogranite, to leucomonzogranite and leucogranite, reflecting a significant range of whole-rock silica content. Texturally, samples are either coarse- to fine-grained equigranular or porphyritic, with phenocrysts of either quartz or K-feldspar. Grains were usually 0.5 - 5 mm in size, while phenocrysts were up to 5 cm in size. Additional rock descriptor terms used are based on the identity of the mica present as well as grain size. Table 1 summarizes the mineralogy and textures for all samples, and full petrographic descriptions of each sample are available in Appendix A.

The most abundant minerals in the samples are quartz (~20-30%), plagioclase (~25-40%), K-feldspar (~20-40%), with the amount of biotite decreasing from granodiorite (~15%) through to leucogranite (≥1%). The abundance of muscovite is highest in the leucogranites (~1-5%) and decreases to trace levels through to granodiorite compositions. Muscovite usually appears as a secondary phase in the samples. Common accessory minerals include apatite, zircon, ilmenite, rutile, and monazite, which are most easily detected as inclusions within biotite grains. Apatite grains could be up to ~0.2 mm in size, while other accessory minerals tended to be smaller. Elongated ilmenite was also commonly located along cleavages of the biotite grains.

Clarke et al. (2022) discusses the textural association between biotite and its inclusions and has shown that for samples from the Halifax pluton of the SMB, there is a preferential concentration of accessory minerals in biotite compared to any other major rock-forming mineral. The origin of this unique association is concluded by Clarke et al. (2022) to be related to a combination of factors, including chemical affinity, diffusion pileup and the relative timing of crystal growth. The abundance of biotite-hosted accessory minerals is generally higher in samples from the SGP than the NRP (Figure 6), which reflects a more general observation of a higher accessory mineral inclusion density in Stage 1 vs Stage 2 biotite.

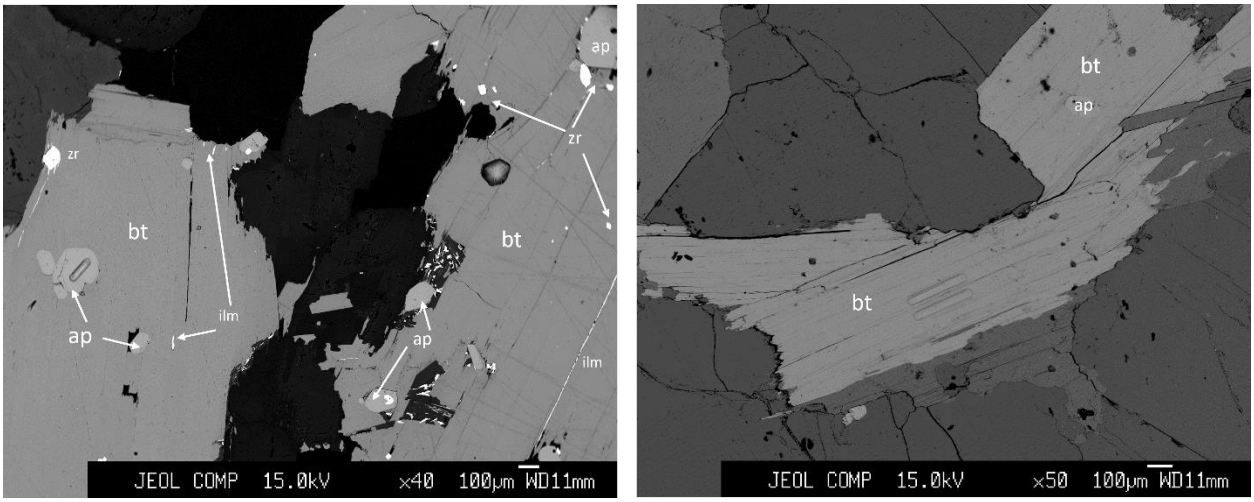

Figure 6 – Two back scatter electron (BSE) images comparing the frequency of inclusions in biotites (bt) in two samples. The left image is from a Stage 1 SGP sample, 19BM-0004, while the right image is from a Stage 2 NRP sample, A16-1171. The Stage 1 sample contains abundant inclusions of apatite (ap), ilmenite (ilm), and zircon (zr), while the Stage 2 sample only contains a single apatite inclusion. The surrounding darker material in the images are quartz, plagioclase, and feldspar.

The biotite grains range from euhedral to anhedral and are generally more euhedral in the less evolved samples (i.e., granodiorite-monzogranite). Biotite grains also showed varying levels of alteration to chlorite, usually along the grain edges and cleavages. The level of alteration, from least (0) to complete replacement (2) is summarized in Table 1. Biotite grains are usually located amongst larger plagioclase and K-feldspar grains, suggesting it forms later in the crystallization sequence. The larger grains and more euhedral shapes of biotite in less evolved samples, especially SGP samples, suggests that they form earlier compared to biotites in more evolved samples.

Table 1 - Summary of samples

Sample	Texture	Easting	Northing	Lithology	Pluton	Phase	Grain Size	Modal % Biotite	Degree of Chloritization	Frequency of Inclusions In Biotite
19BM-0004	Equigranular	348166	4948721	BGD	SGP	1	MG	15	0	2
A09-2378	Equigranular (Excluding Biotite)	397167	4948103	CGLMG	NRP	2	CG	3	1	3
A10-3020	Equigranular	378162	4937604	CGLMG	NRP	2	CG	2	1	2
A10-3106	Porphyritic K-Feldspar	346510	4952014	BGD	SGP	1	CG	15	1	3
A11-2268	Equigranular	303819	4949639	FGLMG	SGP	1	FG to MG	3	0	1
A11-2282	Equigranular	322790	4945121	MLG	SGP	1	FG	1	0	1
A12-1015	Porphyritic Quartz	300937	4949316	BGD	SGP	1	MG to CG	15	1	3
A12-8007	Porphyritic K-Feldspar	294849	4950294	BGD	SGP	1	CG	15	1	3
A15-0102	Porphyritic K-Feldspar	357098	4957453	FGLMG	SGP	1	FG to MG	4	1	2
A15-0114	Equigranular	342670	4961750	FGLMG	SGP	1	FG to MG	1	2	1
A16-1171	Equigranular	405875	4964951	CGLMG	NRP	2	MG	1	1	1
A16-1174	Porphyritic K-Feldspar	408258	4961032	CGLMG	NRP	2	MG	3	1	2
A16-1256	Equigranular	392565	4960613	MLG	NRP	2	MG to CG	5	0	2

BGD= Biotite Granodiorite; BMG= Biotite Monzogranite; MBMG= Muscovite Biotite Monzogranite; CGLMG= Coarse-grained Leucomonzogranite; FGLMG= Fine-grained Leucomonzogranite; MLG= Muscovite Leucogranite
NRP= New Ross Pluton; SGP= Scrag Lake Pluton

Degree of Chloritization

0) Negligible: No alteration to one or two grains with minor alteration on grain boundaries
1) Minor alteration: Most grains have alteration on grain boundaries or a few grains have been completely replaced by chlorite
2) Significant alteration: Almost all grains have alteration with multiple grain being completely altered. Less then half of the Biotite grains have ben altered to chlorite
3) Widespread alteration: Almost no Biotite remains

Frequency of Inclusions

1) Rare: One or two grains have inclusions
2) Uncommon: Less then 2/3 the grains have inclusions
3) Common: Almost all grains have them or a few grains have multiple of inclusions
4) Abundant : All grain have multiple inclusions

CG: Coarse grained (>2 mm)
MG: Medium grained (1-2mm)
FG: Fine Grained (<1 mm)

Coordinates are in UTM 20 NAD 83

4.2 Major element composition of biotite

The major element composition of biotite determined by electron microprobe is provided in Table B1 of the Appendix. Figure 7 compares the abundance of select major elements in NRP and SGP samples as a function of the biotite TiO_2 concentration. The abundance of TiO_2 in the biotite is chosen as an indicator of sample differentiation, with high TiO_2 compositions being less evolved. As can be seen from the data, there are no significant differences in biotite compositions between the two suites. This is consistent with the overlap in whole-rock major element compositions.

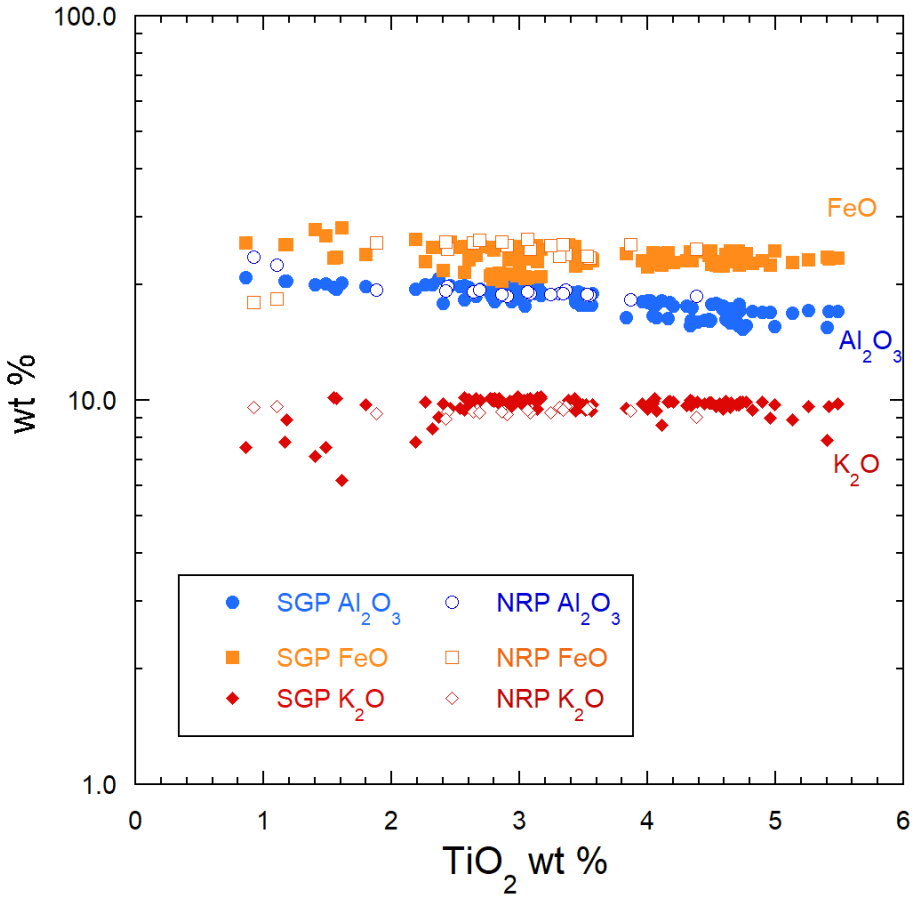

Figure 7 – Plot of major element concentrations as a function of TiO_2 concentration for SGP and NRP biotites. Stage 1 samples have filled symbols and the Stage 2 samples have open symbols. This shows that the major element overlap observed in the whole rock data between the two phases of the SMB is reflected in the biotite compositions.

The biotite major element data were also used to calculate the mineral stoichiometry expressed as the number of atoms of each element in the biotite chemical formula based on 22 oxygens per formula unit. Results of these calculations are in included in Table B1 and portrayed in Figure 8 in terms of the total tetrahedral aluminum, ^{IV}Al, as a function of Fe/(Fe+Mg) (or the Fe#). According to this Figure, the biotites are classified as siderophyllite to annite. As per the major element comparison, most of the SGP and NRP samples overlap in terms of the ^{IV}Al-Fe# variation and are similar in composition to biotite from other peraluminous granites (Clarke, 1981).

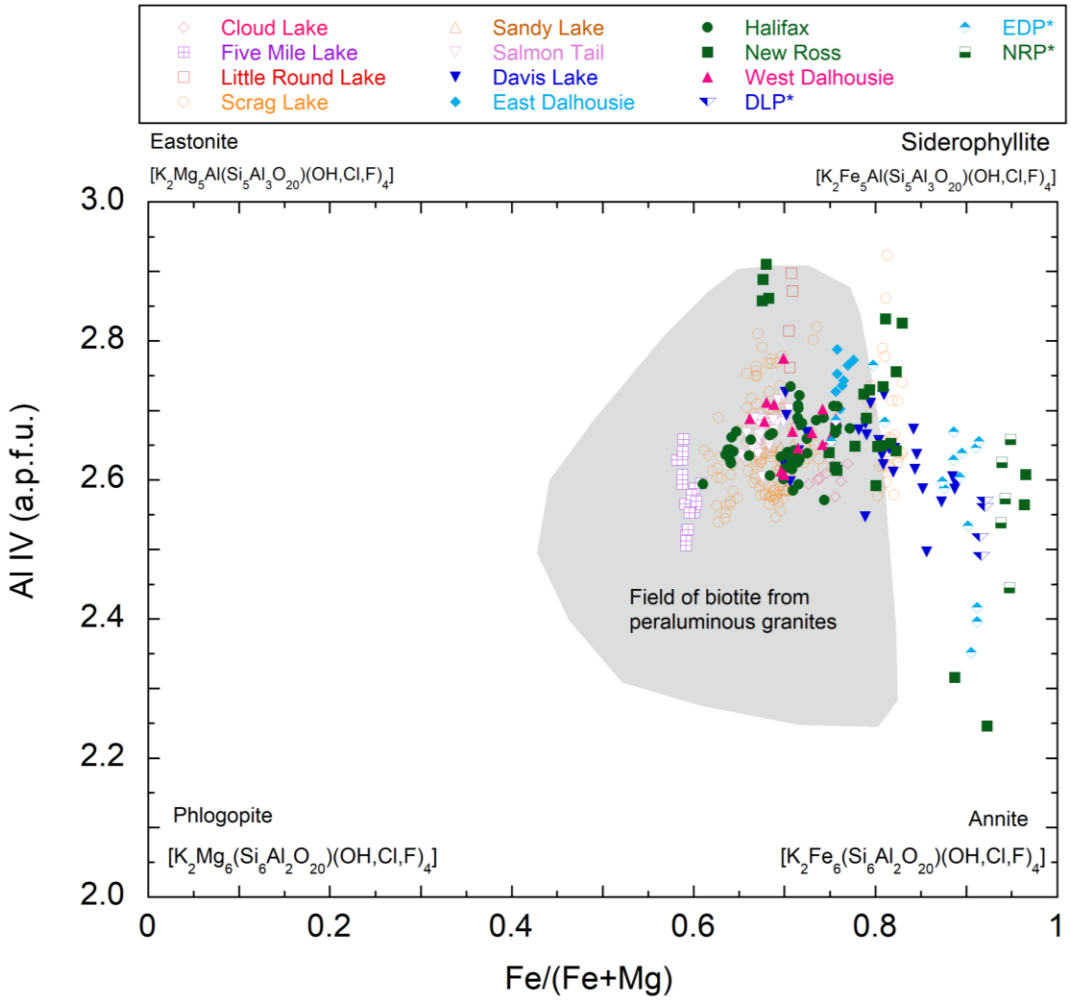

Figure 8 – The biotite classification diagram for all SMB samples based on the proportions of tetrahedral aluminum, Al^{IV}, as a function of Fe/(Fe+Mg), with all values calculated based on 22 oxygens per formula unit. The samples from this study are the Scrag Lake and New Ross samples, which are mostly located in the field of biotite

from peraluminous granites, with a few outliers from NRP plotting with higher Fe# values (Clarke, 1981). The symbols marked as DLP*, EDP* and NRP* are those samples with Nb/Ta < 5.

4.3 Trace element composition of biotite

A total of 34 trace elements were measured using laser ablation ICP-MS for each compositional map, however only 18 of these were consistently at concentrations above detection. The maps were used to classify the nature of the zoning observed, with four categories distinguished based on the nature of the core to rim trace element variation. The most common type of trace element variation observed involves either a continuous increase (category 1) or decrease (category 2) in abundance from core to rim. A third category was identified in which the trace element concentration does not vary across the biotite grain. Finally, a fourth category was distinguished in a few samples in which elements displayed oscillatory zoning. A table describing the type of zoning for each element that was above the detection limit can be found in Appendix C as table C1, and a summary of the elements in each category is provided below. The trace elements for the maps used extensively in this section are located on the next couple of pages as Figures 9 to 12.

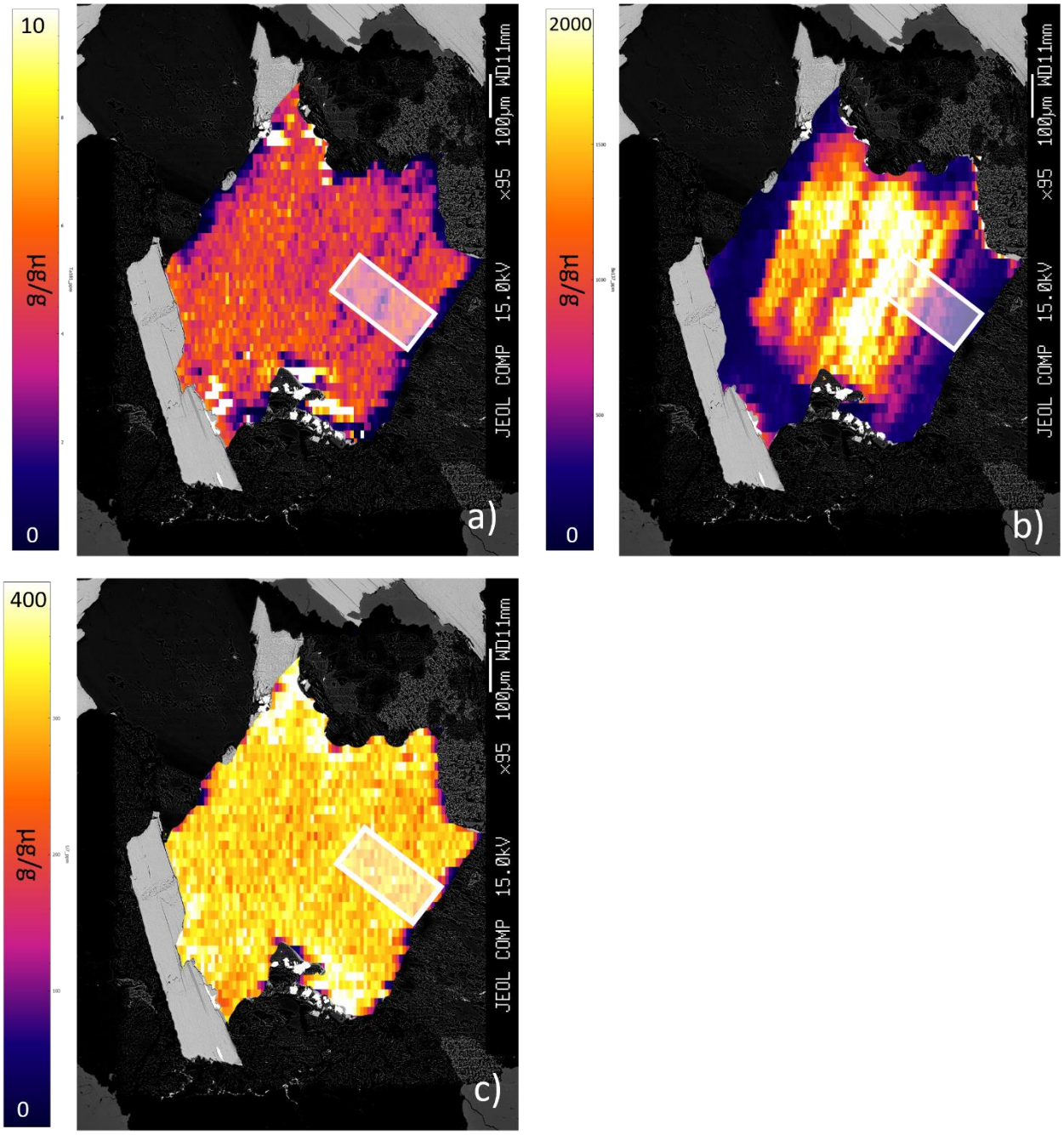

Figure 9 – Trace element maps for sample 19BM-0004 biotite 2, a Stage 1 SGP sample (whole rock SiO_2 = 68.78 wt %), cropped onto BSE images of the biotite grains. A region of interest is highlighted by the white rectangles, and the trace element concentration data from this region is used throughout section 4.3. (a) The Ta trace element map of the sample. (b) The Ba trace element map of the sample. (c) The Li trace element map of the sample.

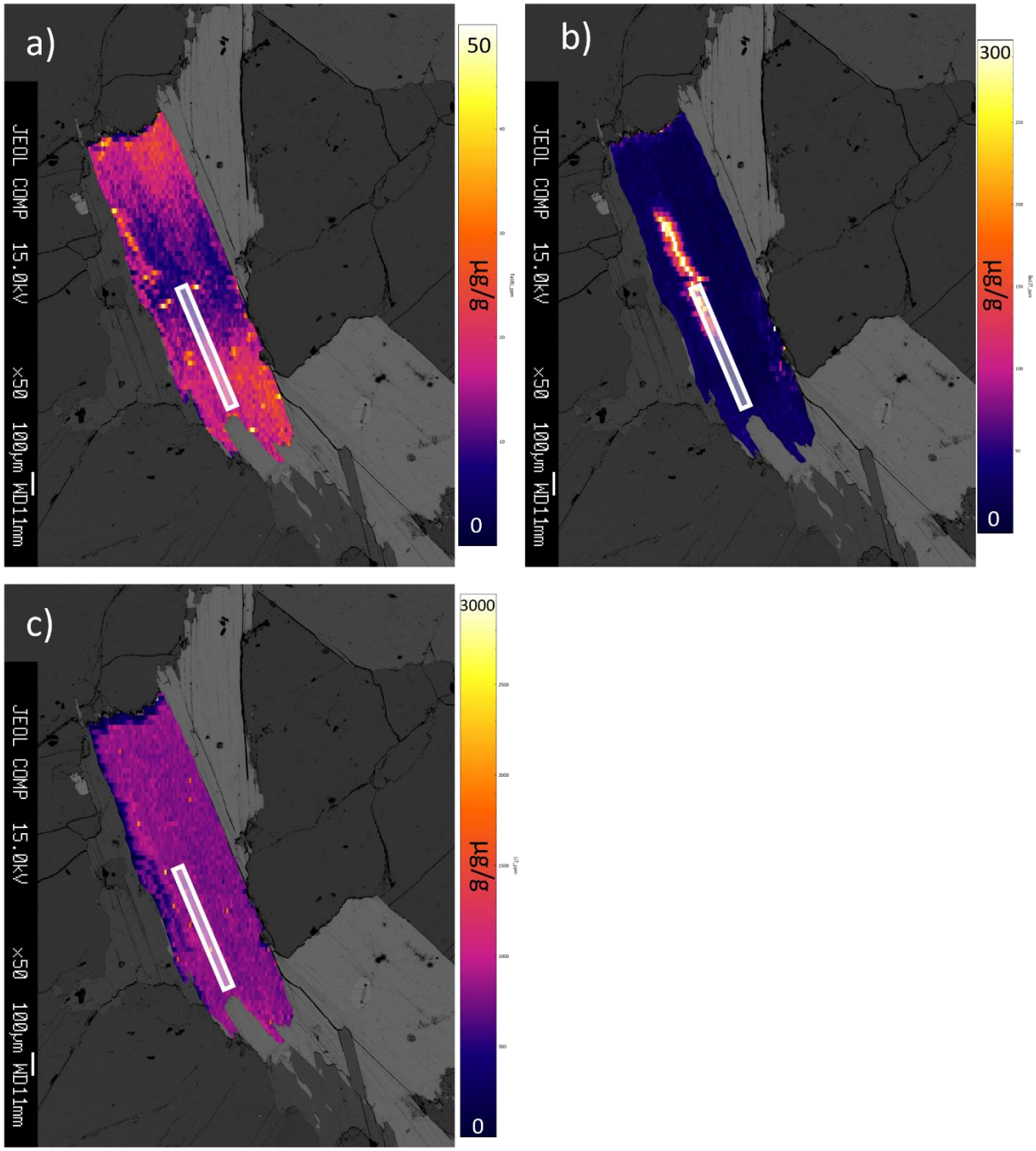

Figure 10 – Trace element maps for sample A16-1171, a Stage 2 NRP sample (whole rock SiO_2 = 69.83 wt %), cropped onto BSE images of the biotite grains. A region of interest is highlighted by the white rectangles, and the trace element concentration data from this region is used throughout section 4.3. (a) The Ta trace element map of the sample. (b) The Ba trace element map of the sample. (c) The Li trace element map of the sample.

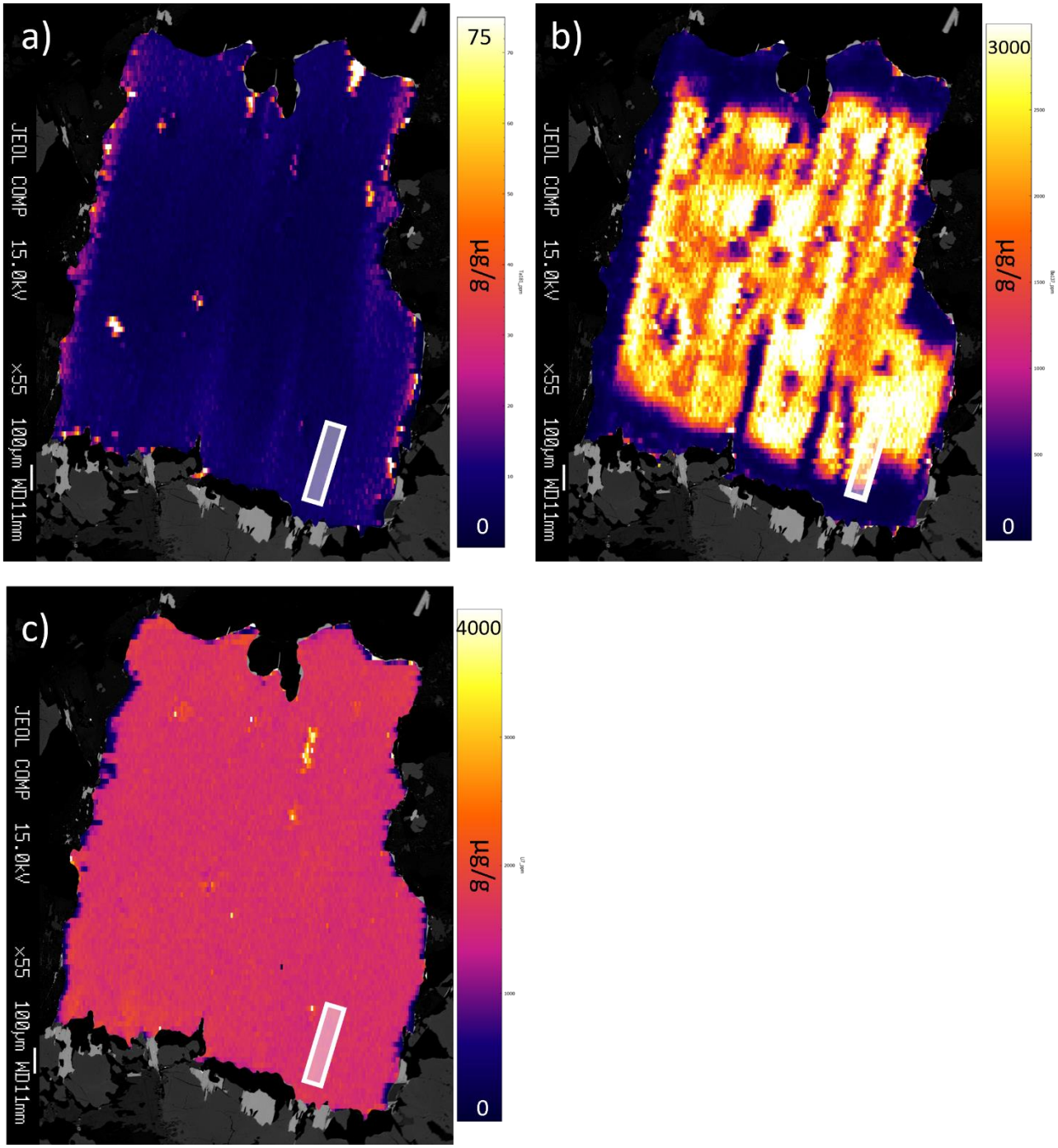

Figure 11 – Trace element maps for sample A11-2268, a Stage 1 SGP sample (whole rock SiO_2 = 74.26 wt %), cropped onto BSE images of the biotite grains. A region of interest is highlighted by the white rectangles, and the trace element concentration data from this region is used throughout section 4.3. (a) The Ta trace element map of the sample. (b) The Ba trace element map of the sample. (c) The Li trace element map of the sample.

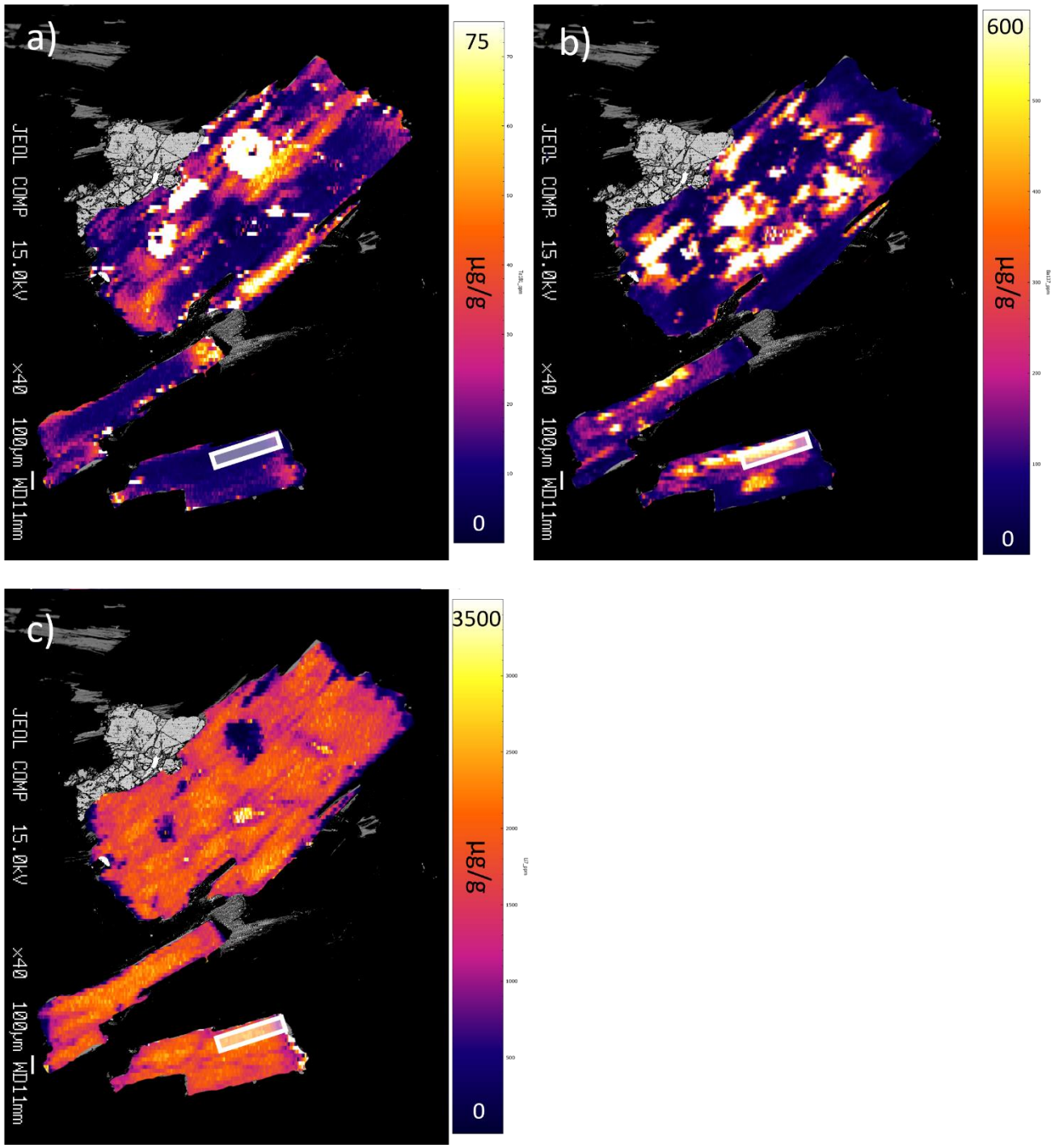

Figure 12 – Trace element maps for sample A10-3020, a Stage 2 NRP sample (whole rock SiO_2 = 73.12 wt %), cropped onto BSE images of the biotite grains. A region of interest is highlighted by the white rectangles, and the trace element concentration data from this region is used throughout section 4.3. (a) The Ta trace element map of the sample. (b) The Ba trace element map of the sample. (c) The Li trace element map of the sample.

4.3.1 Continuously Increasing Zoning

The elements that showed continuously increasing concentrations from core to rim, which is interpreted to signify over all incompatibility in the crystallizing assemblage, are Rb, Nb, Sn, Cs, Ta, and W. As an example, the trace element maps for Ta are shown in Figures 9a, 10a, 11a, and 12a. In general, zoning of this type tended to show greater element variation in more evolved samples compared to less evolved samples. Concentrations were also higher in samples from the NRP compared to those from the SGP.

Figure 13 compares the core-to-rim concentrations of Ta concentrations for samples with similar whole-rock SiO_2 content. The NRP samples show higher concentrations, and greater degree of change from core to rim compared to the SGP samples. When the Ta concentrations from these maps are added to Figure 14, we can see that the stage 1 "Composition Gap" has been filled in more and that Ta does not vary in Stage 1 to the same degree as Stage 2.

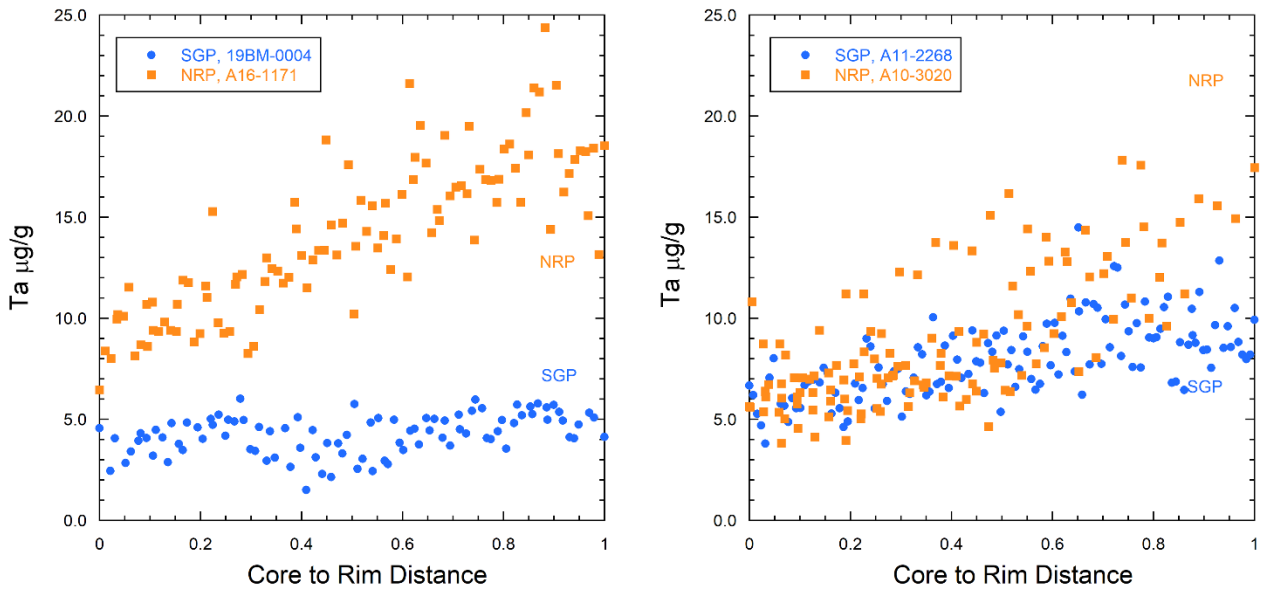

Figure 13 – Plots comparing the Ta concentrations in less evolved samples (left) and in more evolved samples (right). Concentrations are plotted against the normalized core to rim distance across an area of zoning in each grain, and these areas are outlined on Ta maps in Figures 9a, 10a, 11a, and 12a.

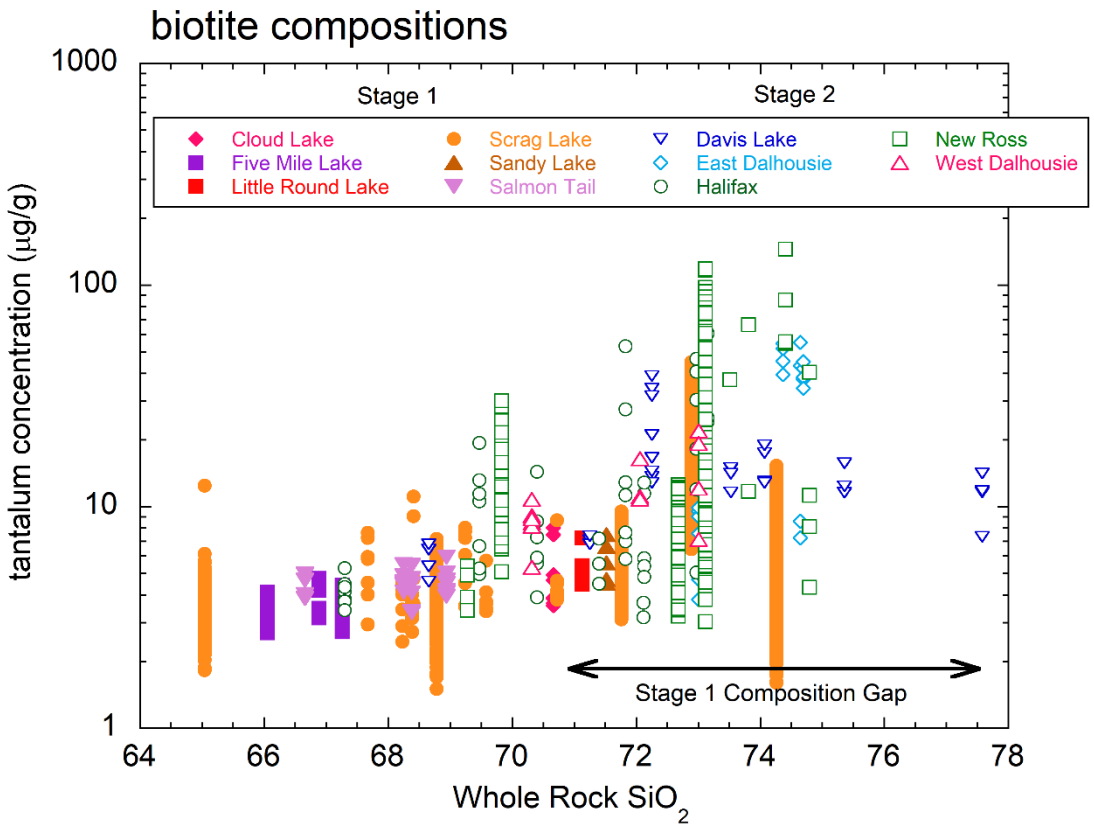

Figure 14 – An updated version of Figure 1 including newly acquired Ta concentration data from all Stage 1 SGP and Stage 2 NRP samples, filling in the Stage 1 Composition Gap. This new data shows that Ta variability in Stage 1 samples is usually 1 – 10 µg/g, with one outlier showing variability from 10 – 30 µg/g. This is still less variation than the Stage 2 samples.

4.3.2 Continuously Decreasing Zoning

The elements that showed continuously decreasing concentrations from core to rim, which is interpreted to reflect compatibility in the crystallizing assemblage, are Sc, Ti, V, Cr, Ga, and Ba. As an example, the trace element maps for Ba are shown in Figures 9b, 10b, 11b, and 12b, and the core-to-rim variations in Figure 15. In general, the maps reveal a larger concentration variation in the less evolved samples from either pluton and higher overall concentrations in biotite from the SGP.

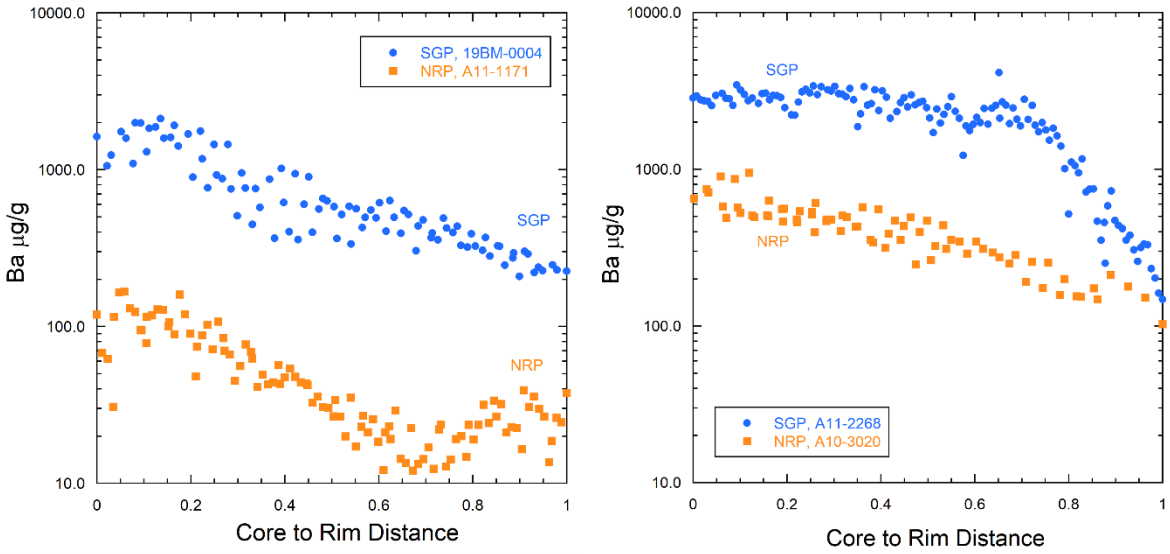

Figure 15 - Plots comparing the Ba concentrations in less evolved samples (left) and in more evolved samples (right). These concentrations are plotted against the normalized core to rim distance across an area of zoning in each grain, and these areas are outlined on Ba maps in Figures 9b, 10b, 11b, and 12b.

4.3.3 Constant Concentrations

The elements that did not show any zoning and instead showed uniform core-to-rim concentrations (implying bulk mineral-melt partition coefficients of near unity) are Li, Mn, Fe, Co, Ni, and Zn. While the concentrations were constant across a given biotite grain, trace element levels did show differences between different samples. For example, Li concentrations are higher in more evolved samples (see Figure 16), while Mn, Fe, Co, Ni, and Zn all showed lower concentrations in more evolved samples. In a few select cases, Li (Figure 17), Co, and Zn showed weak zoning towards the edges of the biotite grains (for more details as to which samples display this, see Appendix C).

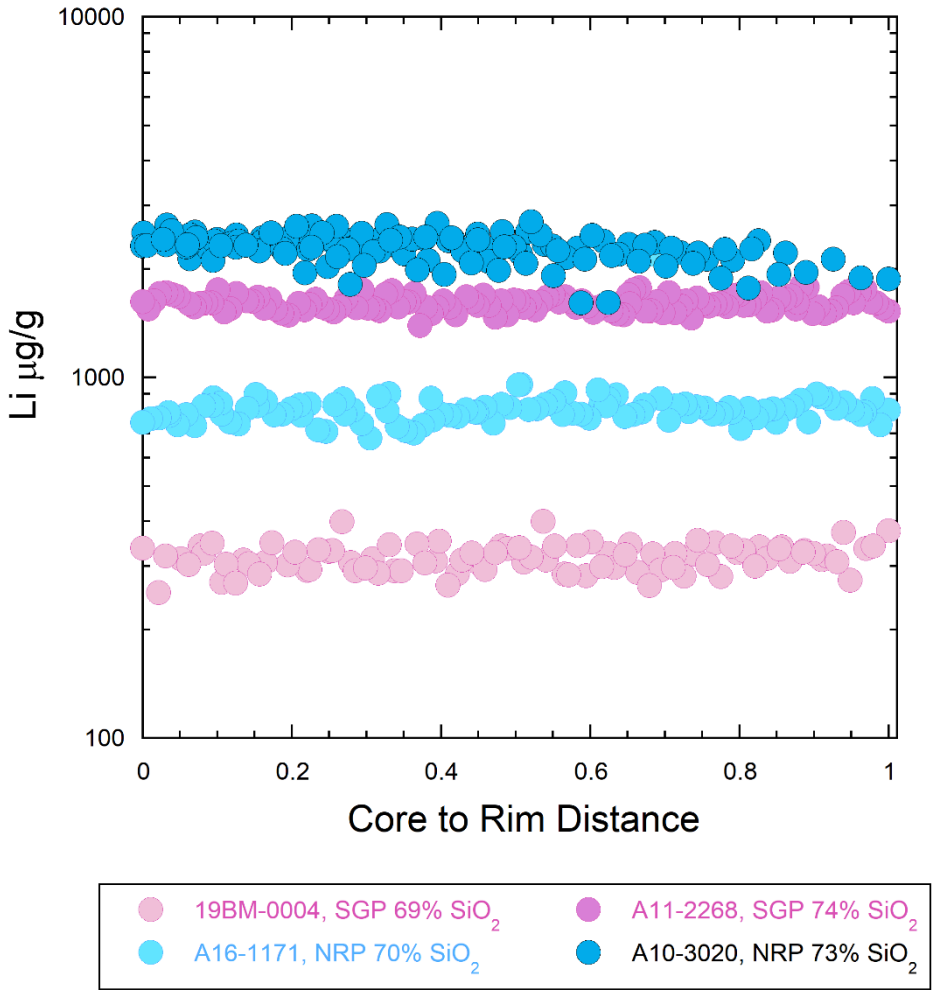

Figure 16 – Plot comparing the Li concentrations in low and high SiO_2 samples from both SGP and NRP. These concentrations are plotted against the normalized core to rim distance across an area of zoning in each grain, and these areas are outlined on Li maps in Figures 9c, 10c, 11c, and 12c.

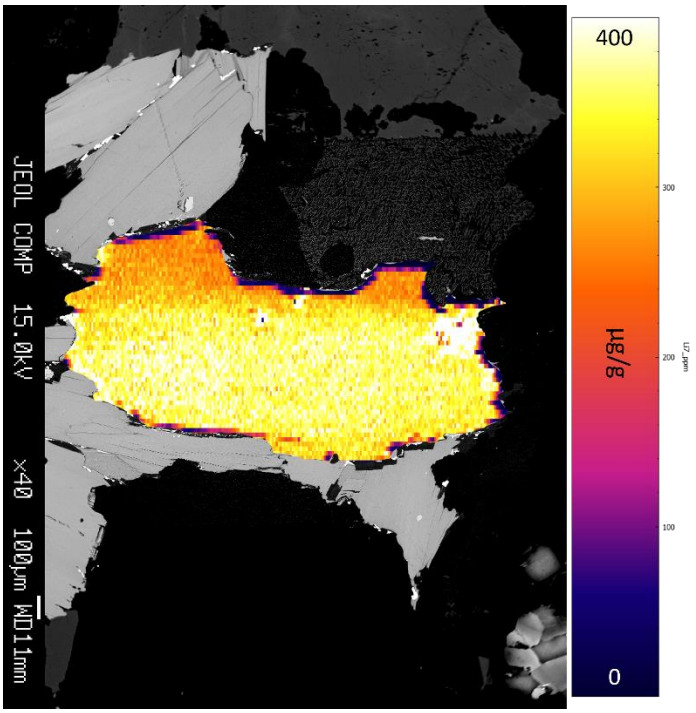

Figure 17 – An example of weak Li zoning in Stage 1 sample 19BM-0004 biotite 1, seen towards the top edge of the grain. The Li trace element map has been cropped onto an BSE image of the grain.

4.3.4 Oscillatory Zoning

Two of the least evolved samples from the SGP, 19BM-0004 (biotite 1) and A12-8007, showed oscillatory zoning in the concentrations of Ba and Ga. The maps of these samples are shown in Figures 18 and 19, and core-to-rim concentrations in Figure 20. Both elements display the same oscillatory trends, with an initial decrease, suggestive of compatible behaviour during crystallization, then an abrupt increase to approximately the initial concentrations, followed by a further decrease to below the level of the previous abrupt increase.

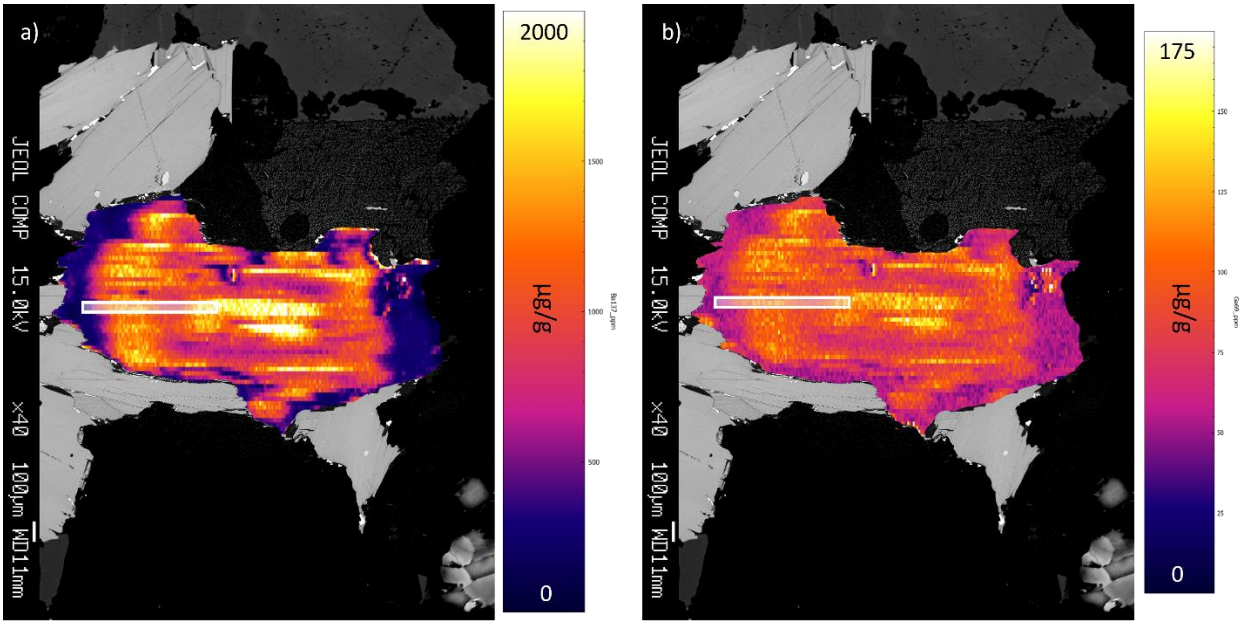

Figure 18 – The trace element maps for Stage 1 sample 19BM-0004 biotite 1 (whole rock SiO_2 = 68.78 wt %), cropped onto an BSE of the grain. A region of interest is highlighted by white rectangles, and the trace element concentration data from these regions is plotted in Figure 20. (a) The Ba trace element map of the sample. (b) The Ga trace element map of the sample.

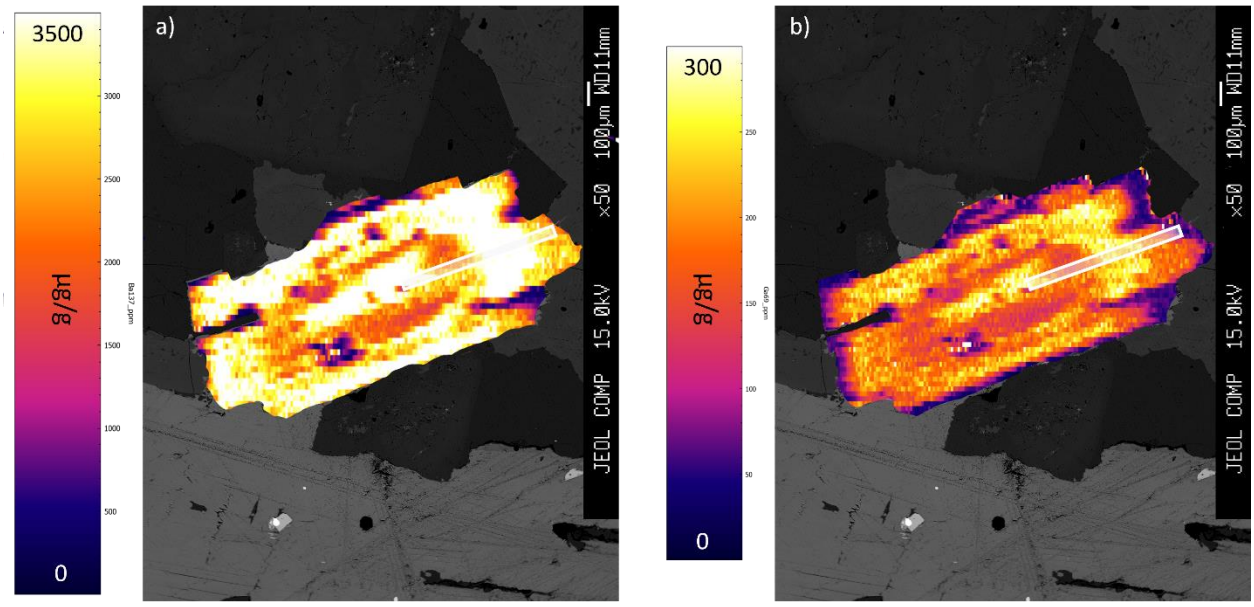

Figure 19 – The trace element maps for Stage 1 sample A12-8007, (whole rock SiO_2 = 65.04 wt %), cropped onto an BSE of the grain. A region of interest is highlighted by white rectangles, and the trace element concentration data from these regions is plotted in Figure 20. (a) The Ba trace element map of the sample. (b) The Ga trace element map of the sample.

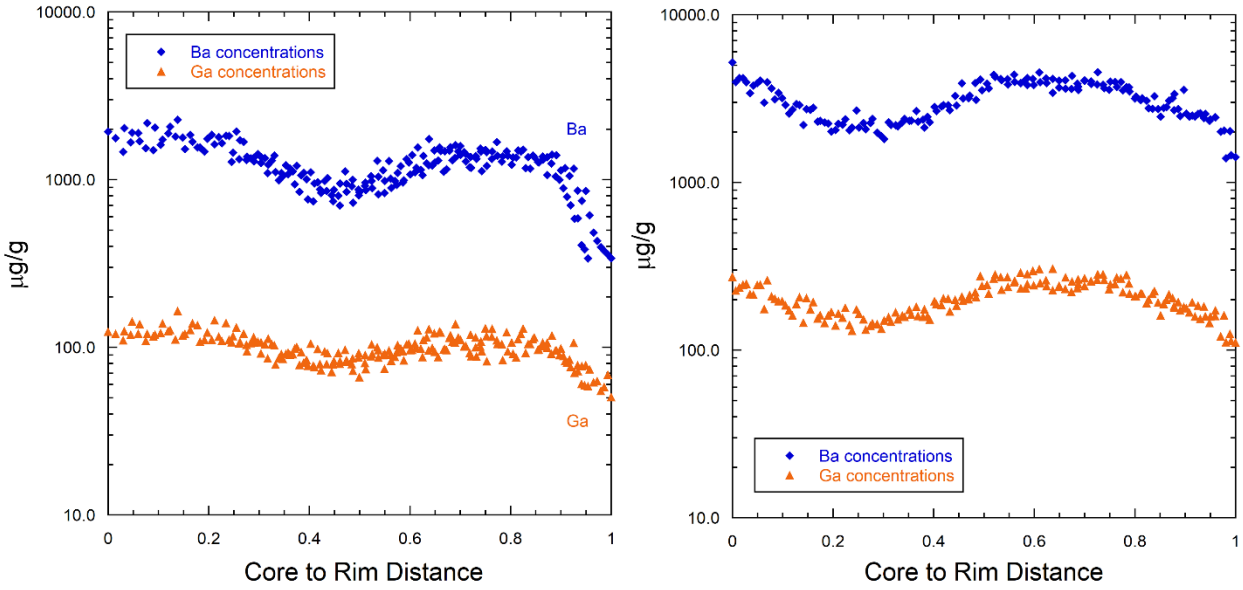

Figure 20 - Plots comparing the Ba (blue) and Ga (orange) concentrations in 19BM-0004 (left) and in A12-8007 (right). These concentrations are plotted against the normalized core to rim distance across an area of zoning in each grain, and these areas are outlined in Figures 18 and 19.

4.4 Anion chemistry

Variation in the anion concentration (F, Cl and OH) of biotite is potentially a useful indicator of the development of a magmatic vapour phase during crystallization, owing to differences in melt/vapour partitioning of F (melt compatible) and Cl (vapour compatible; Baker and Alletti, 2012). Both F and Cl were measured by electron microprobe, and although the abundance of hydroxyl in biotite was not measured directly, amounts can be estimated by mineral stoichiometry. For both sample suites, the mole fraction of the anion site occupancy decreases in the order OH (2.5-3.5 apfu), followed by F (0.1-1.1 apfu) and Cl (<0.05 apfu). In comparison, samples from the SGP have lower F and higher OH than those from the NRP, with similar levels of Cl in each. The variation in anion site occupancy as a function of the biotite TiO_2 concentration, a measure of differentiation (see start of Section 4.2), is portrayed in Figure 21.

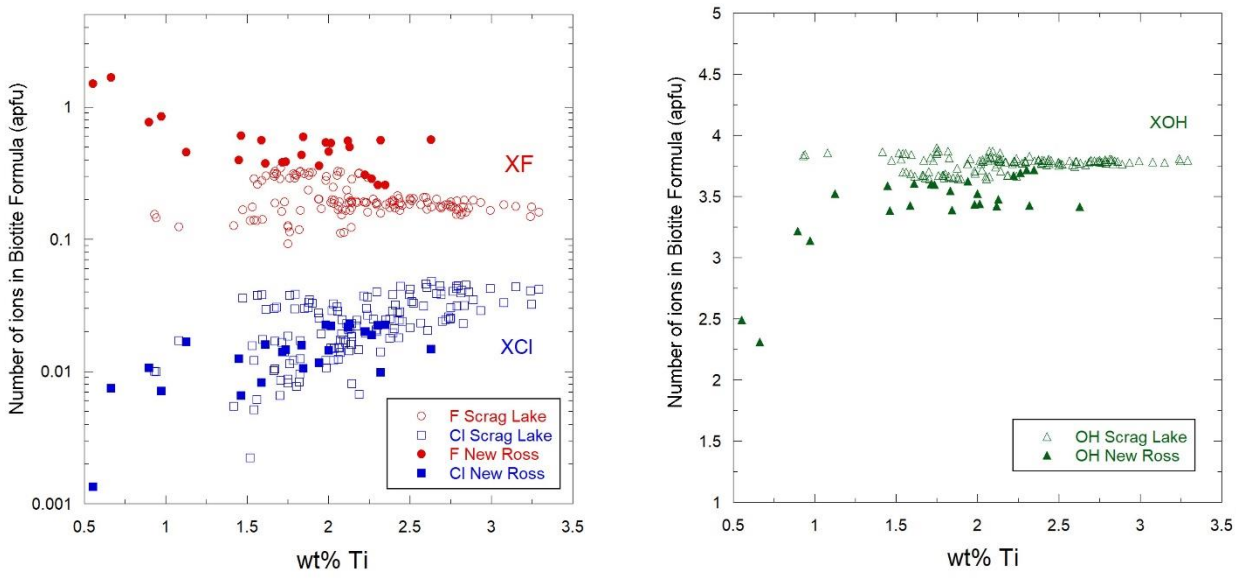

Figure 21 – Plots of the anion mole fractions versus the biotite TiO_2 wt% for all samples in this study. Open symbols are for Stage 1 SGP samples while the closed symbols are for the Stage 2 NRP samples. The left plot shows the mole fractions for F and Cl, while the right plot shows the OH mole fractions.

The data shows that the OH concentration in biotite is relatively constant (~3.75 apfu) with changing TiO_2 for samples from the SGP, whereas samples from the NRP show OH decreasing from 3.75 to 2.5 apfu as TiO_2 decreases. Fluorine shows similar behaviour to OH in the SGP samples, in terms of little variation (~0.1-0.2 apfu) with changing TiO_2, whereas F concentrations in samples from the NRP increase from 0.1 to 1.1 apfu with decreasing TiO_2. Finally, both SGP and NRP samples show decreasing amounts of Cl from 0.05 to 0.001 apfu as TiO_2 decreases.

5.0 Discussion of Results

5.1 Geochemical Trends

Figure 7 show that the biotite major element data follows similar trends to the whole rock major element data (Figure 3). The biotite major element data also shows little difference between the SGP and NRP samples, consistent with the similarity in whole rock major element data between Stage 1 and Stage samples. As well, the biotite samples from this study mostly plot in the peraluminous field in the biotite classification diagram in Figure 8. As such, the biotite major element data collected is consistent with expectations.

From the trace element maps, it can be concluded that Rb, Nb, Sn, Cs, Ta, and W are all behaving incompatibly during sample crystallization. Each of Rb, Ta, Sn, and W in particular are mirroring the whole rock trend noted previously for the entire SMB dataset, with concentrations increasing as SiO_2 increases (Macdonald et al., 1992). As Figures 13 and 14 illustrate, Ta concentrations vary on smaller scales (1-10 μg/g) compared to Stage 2 samples. This suggests that the differences initially seen in trace element concentrations between phases are not due to sampling biases, but are instead an inherent feature of the SMB. The enrichment of an ore metals like Ta, Sn, and W in Stage 2 is also important to note as this means Stage 2 plutons would be more likely to host potential ore deposits of these elements than Stage 1 plutons.

In contrast, Sc, Ti, V, Cr, Ga, and Ba are behaving compatibly in the biotite samples. The elements Ti, Ba, Sc, and V are also mirroring the whole rock trends for the SMB dataset, showing decreasing concentrations as SiO_2 increases (Macdonald et al., 1992). All these trace elements are also behaving in biotite grains as previously described in samples from across the SMB (Brenan et al., in preparation).

The elements that do not show zoning in the biotite samples, Li, Mn, Fe, Co, Ni, and Zn, do show differences between different samples (Figure 16). This is unexpected, as a uniform concentration in the biotite grains would imply a bulk partitioning coefficient of 1 in these samples, and thus there should be no difference in concentration between them. One possibility is that the elements may indeed have been zoned during crystal growth, but there

was enough time for the elements to diffuse through the biotite and thus remove the zonation since the mineral crystallized. This idea is supported by the Li, Co, and Zn maps that do display weak zoning. Although there are limited data for diffusion of cations in biotite, Hammouda and Cherniak (2000) documented relatively rapid diffusion of Sr in fluorphlogopite perpendicular to the c-axis. Results suggest a closure temperature for Sr exchange of ~400°C. If these results are applicable to other divalent cations, then it seems likely that gradients produced during crystallization at high temperature could be partially to completely removed during lower temperature annealing. With the exception of Ba, Rb and Cs, the elements that preserve compositional zoning in biotite are all more highly charged than 2+, with higher charge usually resulting in slower diffusion (Cherniak and Diminov, 2010), and the likelihood of preserving concentration gradients.

5.2 Modelling of Biotite Zoning Patterns

In order to evaluate whether the variation in trace element abundances from biotite maps are consistent with normal crystallization processes, model crystallization curves were calculated and compared with the observed core-to-rim gradients. To do this, model liquid concentrations, C_L, were calculated from the equation for fractional crystallization:

$$C_L = C_o F^{(D_i{}^{bulk}-1)} \qquad (1)$$

in which C_o is the initial liquid composition, F is the fraction of liquid remaining and $D_i{}^{bulk}$ is the bulk solid/liquid partition coefficient, which is defined as:

$$D_i{}^{bulk} = \sum X_{mineral}\, D_i{}^{mineral/liquid} \qquad (2)$$

This is the sum of the individual mineral/melt partition coefficients, $D_i{}^{mineral/liquid}$, for an element *i*, multiplied by the mass fraction of each mineral, $X_{mineral}$, in the crystallizing assemblage. Concentrations in the liquid were then converted to concentrations in coexisting biotite, $C_{biotite}$, using the relation:

$$C_{biotite} = D^{biotite/melt} C_L \qquad (3)$$

in which $D^{biotite/melt}$ is the biotite/melt partition coefficient.

The model crystallizing assemblage consists of 31-39% quartz, 20-25% K-feldspar, 39-42% plagioclase and 1-10% biotite, which is based on the normative mineralogy of average SMB biotite granodiorite from MacDonald et al. (1992). The data chosen to compare against this model is that of a representative compatible and a representative incompatible element (with respect to the crystallizing assemblage). The designation of element behaviour is based on the change in element concentration compared to whole-rock SiO_2 and with core-to-rim variations. Ba is considered to be compatible as whole-rock concentrations decrease with increasing SiO_2, and concentrations in biotite decrease from core to rim. The opposite behaviour is shown for Ta, in which concentrations increase in both cases. The quartz-melt partition coefficients are assumed = 0 for both elements, as is the $D^{Feldspar/melt}$ for Ta. Values for other minerals, summarized in Table 2, are estimated from coexisting mineral and glass from the Fish Canyon and Toba tuffs (Bachmann et al., 2005; Maciag et al., 2021), which are rapidly-quenched volcanic rocks. Estimates of the initial liquid concentration, C_o, are based on whole rock Ba- and Ta-SiO_2 variations. A summary of model parameters is provided in Table 2.

Table 2 - Summary of parameters used in modelling

parameter	value
C_o^{Ta}	1.6 µg/g
C_o^{Ba}	700 µg/g
$D_{Ta}^{biotite/melt}$	1.7
$D_{Ba}^{biotite/melt}$	5.5
$D_{Ba}^{K\text{-}spar/melt}$	17
$D_{Ba}^{plag/melt}$	0.6

The models produced were then plotted against the Ba and Ta concentrations used to create Figures 13 and 15. This way, the models were compared to less-evolved and more-evolved samples with similar SiO_2 contents from both SGP and NRP. The plot of the data and the models are provided in Figure 22.

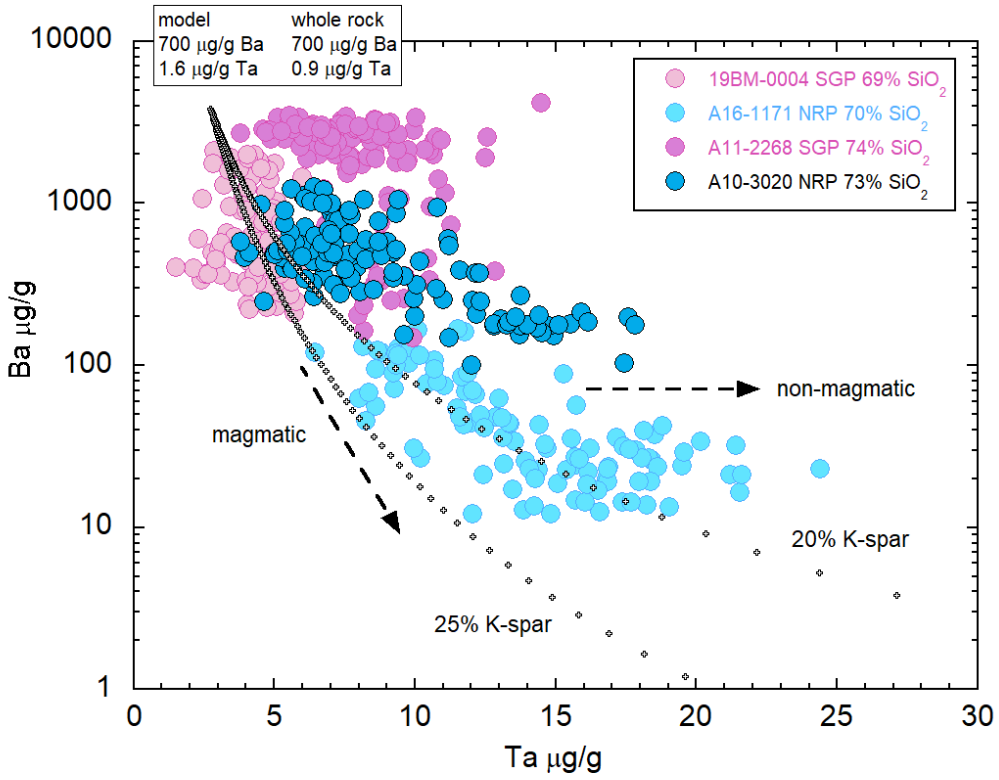

Figure 22 – Plot of the Ba as a function of Ta concentrations for SGP and NRP biotite and model crystallization curves. There are two models plotted on the graph, one for crystallization with modal abundances of 25% K-feldspar, 31% quartz, 42% plagioclase, and 2% biotite (steeper model curve). The second uses 20% K-feldspar, 39% quartz, 39% plagioclase, and 2% biotite (curve to the right). The models start at 0% crystallization in the upper-left corner and show increasing crystallizing towards the bottom-right. The model starting concentrations for Ta and Ba, and measured whole rock concentrations for Ta and Ba are listed in the upper left part of the plot. The plot is also labeled to show magmatic and non-magmatic trends, showing that the samples with higher Ta concentrations are following a non-magmatic trend.

Figure 22 shows that while the models do follow the general trend of the data, there is a clear horizontal trend for higher Ta samples that cannot be explained by the simple crystallization model alone. This would suggest that a non-magmatic process, such as hydrothermal activity, may be affecting these samples. This modeling also shows that more evolved samples plot further along the model curve (i.e. at lower Ba and higher Ta concentrations) than less evolved samples. The model also suggests that the NRP samples are

crystallizing from a more evolved melt, and thus may be crystallizing at a later point compared to the SGP samples.

It is also important to note that the measured whole rock C_o^{Ta} value, 0.9 µg/g, is lower than the value used in the model, which might suggest that the whole rock data may not be an appropriate representation for the liquid.

While the 20% K-feldspar model does model the Ta-rich data better than the 25% K-feldspar model, this does not reflect the observed modal abundances of the samples. There are usually higher amounts of K-feldspar in the more evolved Stage 2 samples, so this further illustrates that fact that there is a non-magmatic process affecting the NRP samples.

5.3 Oscillatory zoning in Ba and Ga

The oscillatory zoning in samples 19BM-0004 biotite 1 and A12-8007 are only seen in 2 of the 18 mapped trace elements, which suggests that the zoning patterns are not due to the melting and recrystallization of the biotite grains themselves. Instead, this oscillatory zoning could be explained by considering another mineral, K-feldspar. Ba does preferentially partition into feldspar compared to biotite (see D_{Ba} values for both minerals in table 2). Ga similarly partitions into K-feldspar (Macdonald et al., 2010). This means that the growth of K-feldspar crystals could lead to lower concentrations of Ba and Ga in biotite as crystallization progresses. However, if the K-feldspar crystals were to melt or dissolve even slightly, this could release Ba and Ga back into the melt, which could result in increasing concentrations in biotite as illustrated in Figure 23.

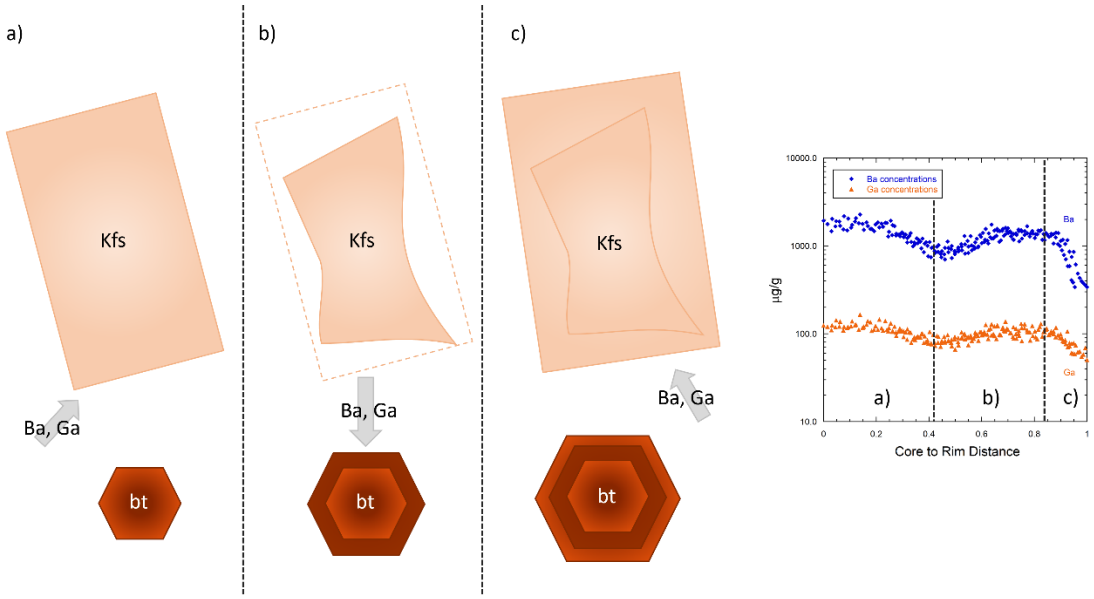

Figure 23 – A diagram showing a potential explanation for the oscillatory zoning of Ba and Ga seen in a few samples. (a) To start, a K-Feldspar grain (Kfs) and a biotite grain (bt) grow simultaneously, and the K-feldspar preferentially incorporates Ba and Ga into its structure, resulting in decreasing concentrations of Ba and Ga in the biotite. (b) The K-feldspar dissolves, releasing Ba and Ga into the melt. These elements are then incorporated by biotite, resulting in increasing concentrations of Ba and Ga in the biotite. (c) The K-feldspar begins to regrow and incorporated Ba and Ga again. This results in the two element's decreasing concentrations in the biotite.

Partial melting or dissolution of the K-feldspar could occur by magma mixing, and evidence of mixing and partial melting of feldspar grains has been previously noted in the SMB, as seen in Figure 24 (Stashin, 2017). This type of oscillatory zoning in Ba and Ga is only seen in the less-evolved members of the SGP, but the previous work done by Stashin (2017) shows K-feldspar dissolution in a Stage 2 pluton. Thus, this type of oscillatory zoning occurring in biotite is likely due to localized dissolution of K-feldspar and is not an inherent feature of any particular Stage or pluton of the SMB. However, more research into investigating K-feldspar dissolution and oscillatory zoning in biotite in the SMB needs to be done investigate this idea further.

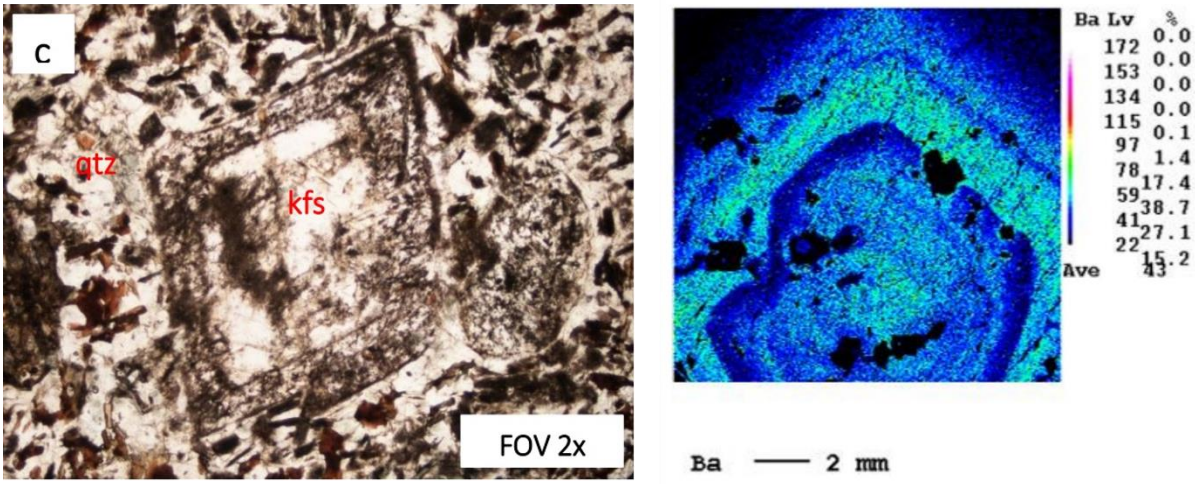

Figure 24 – Previous evidence of K-feldspar dissolution in the SMB found by Stashin (2017). The left image shows a K-feldspar grain (kfs) with a darker dissolution rim around it, surrounded by quartz (qtz). The right image shows oscillatory Ba zoning in a K-feldspar grain, suggesting multiple phases of dissolution and regrowth (Stashin, 2017).

5.4 Anion Chemistry and Li Implications

It is also important to note the potential influence of Li and F in the NRP samples. The whole rock data shows elevated concentrations of these elements in Stage 2 samples (see Figure 4), and this is reflected in the data collected for this study. The halogen data (Figure 21) shows that F is elevated in the most evolved samples, and the trace element maps show higher Li concentrations in NRP biotites (Figure 16). This means that Li and F could serve as potential fluxing agents in Stage 2 magmas and therefore drive more extensive crystallization in Stage 2 by reducing the solidus temperature, allowing for more extensive crystallization to occur (Chen et al., 2014; Manning, 1981; Pichavant et al., 2016), but more research would have to be done to determine how much influence Li and F are exerting.

As well, we see a decrease in Cl in biotites from both Stages of the SMB (Figure 21). As Cl is vapour compatible (Baker and Alletti, 2012), this could suggest that the Cl is partitioning into a vapour phase. This decrease occurs in more evolved samples, so this potential Cl vapour phase could also be affecting Stage 2 samples in a similar manner to Li and F.

6.0 Conclusion

6.1 Most significant findings and their implications

The primary goal of this study was to collect additional data from a Stage 1 pluton of the SMB to fill in the previously noted Stage 1 "Composition Gap" in terms of the trace element chemistry of biotite from more evolved compositions. This was done by collecting trace element data on biotite from seven samples of the Stage 1 SGP whose whole-rock composition ranged from 65.04 to 74.54 wt % SiO_2. Results were compared to trace element compositions collected from five samples from the Stage 2 NRP. The initial hypothesis was that there should be some incompatible trace element variability in the Stage 1 samples, but not to the same degree as Stage 2 samples. This was shown to be true, with Stage 2 biotite samples showing geochemical variability ranging from 10s-1000s µg/g, while Stage 1 samples tended to show variability ranging from 10s-100s µg/g. As well, it was shown that compatible trace elements showed the opposite trend, as Stage 1 samples tended to have concentrations higher than Stage 2 samples. The enrichment of several ore metals like Ta, Sn, and W in higher SiO_2 wt % Stage 2 samples also means that potential ore formation in the SMB would more likely have occurred in Stage 2 plutons.

Several trace elements do not exhibit zoning, but rather nearly constant concentrations within individual biotite grains, but did so some variation between samples. Although constant concentrations within grains may imply bulk partition coefficients of ~1 for these elements, this is not supported by differences in trace element levels between samples. These differences between samples, as well as weak zoning from these elements in some grains, suggests that the overall lack of zoning is ascribed to diffusional relaxation of primary zoning. Finally, oscillatory zoning in Ba and Ga in some samples suggests that, in addition to fractional crystallization, melting and or dissolution of another mineral rich in these elements, suggested to be K-feldspar, is an additional process affecting these concentrations. Melting or dissolution could result from mixing between primitive and evolved melt compositions, which has shown to be the case in other portions of the SMB.

The trace element data were compared to simple fractional crystallization models, which suggested that there are some trends in more evolved samples that cannot be explained

by magmatic processes. As such, it is likely some other process such as hydrothermal activity is affecting Stage 2 samples.

6.2 Recommendations for Future Studies

One of the unexpected discoveries was that of two compatible trace elements, Ba and Ga, showing oscillatory zoning in some of the least evolved SGP samples. While this is likely the result of K-feldspar crystallizing and remelting/dissolving, potentially due to magma mixing, more research needs to be done. Thus, a recommendation for future study would be to map more biotites, to determine if there are more examples of this oscillatory zoning. K-feldspar grains could also be investigated in these samples for evidence of trace element zoning (and the truncations of it) or for melting along grain boundaries. As well, the field relations near where these samples came from could be investigated for evidence of magma mixing to further support the hypothesis.

Another recommendation is to further investigate the more evolved NRP samples. These show evidence of non-magmatic processes affecting them, so more investigation to determine the exact processes that led to these trends should be done. Hydrothermal activity is one possibility, but the potential of Li and F as fluxes, and the influence of a Cl vapour phase in Stage 2 could also be investigated using experimental methods (Manning, 1981; Pichavant et al, 2016) or more detailed numerical modeling.

Finally, the Stage 1 “Composition Gap” could be filled in even more. More biotites from the more evolved SGP samples could be considered, as the most evolved samples from this study did not have many suitable biotites to collect data from. As well, more evolved samples from other Stage 1 plutons could be investigated.

7.0 References

Azadbakht, Z., and Lentz, D.R. (2020). High-resolution LA-ICP-MS trace-element mapping of magmatic biotite: A new approach for studying syn- to post-magmatic evolution. *The Canadian Mineralogist*, vol 58(3), pp 293-311. doi: 10.3749/canmin.1900101

Bachmann, O., Dungan, M.A. and Busy, F. (2005) Insights into shallow magmatic processes in large silicic magma bodies: the trace element record in the Fish Canyon magma body, Colorado. *Contributions to Mineralogy and Petrology*, vol 149, pp 338-349.

Baker, D.R. and Alletti, M. (2012) Fluid saturation and volatile partitioning between melts and hydrous fluids in crustal magmatic systems: The contribution of experimental measurements and solubility models. *Earth-Science Reviews*, vol 114, pp 298-324.

Ballouard, C., Poujol, M., Boulvais, P., Branquet, Y., Tartese, R., and Vigneresse, J. (2016). Nb-Ta fractionation in peraluminous granites: A marker of the magmatic-hydrothermal transition. *Geology*, vol 44(3), pp 231-234. doi: 10.1130/G37475.1

Ballouard C., Massuyeaua, M., Elburga, M.A., Tappea, S., Viljoena, F., and Brandenburget, J-F. (2020). The magmatic and magmatic-hydrothermal evolution of felsic igneous rocks as seen through Nb-Ta geochemical fractionation, with implications for the origins of rare-metal mineralizations. *Earth-Sciences Reviews*, vol 203, pp 1-31. doi: 10.1016/j.earscirev.2020.103115

Bickerton L., Kontak, D.J., Samson, I.M., Murphy, J.B. and Kellett, D.A. (2019). SHRIMP U-Pb zircon dating of the South Mountain Batholith, Nova Scotia: Timing and duration of crystallization and evidence for inheritance. *In* Targeted Geoscience Initiative: 2018 report of activities (N. Rogers, ed.). *Geological Survey of Canada, Open File 8549*, pp 307-320.

Brenan, J.M., Maciag, B.J., and Hanley, J.J. (In Preparation). Geochemical variation in biotite from the Devonian South Mountain Batholith, Nova Scotia Part 1: Constraints on intensive parameters and the development of a magmatic vapour phase.

Chen, B., Ma, X., and Wang, Z. (2014). Origin of the fluorine-rich highly differentiated granites from the Qianlishan composite plutons (South China) and implications for polymetallic mineralization. *Journal of Asian Earth Studies*, vol 93, pp 301-314.

Cherniak, D.J. and Dimanov, A. (2010) Diffusion in Pyroxenes, Mica and Amphibole. In Zhang, Y. and Cherkiak, D. (eds) *Diffusion in Minerals and Melts*, vol 72(1), *Reviews in Mineralogy and Geochemistry*, pp 641-690.

Clarke, D.B. (1981) The mineralogy of peraluminous granites: A review. *Canadian Mineralogist*, vol 19, pp 3-17.

Clarke, D.B., Renno, A.D., Hamilton, D.C., Gilbricht, S. and Bachmann, K. (2021) The spatial association of accessory minerals with biotite in granitic rocks from the South Mountain Batholith, Nova Scotia. *Geosphere*, vol 18, pp 1-18.

Hammouda, T., and Cherniak, D.J. (2000) Diffusion of Sr in fluorphlogopite determined by Rutherford backscattering spectrometry. *Earth and Planetary Science Letters*, vol 178, pp 339-349.

Henry, D.J., Guidotti, C.V., and Thomson, J.A. (2005). The Ti-saturation surface for low-to-medium pressure metapelitic biotites: Implications for geothermometry and Ti-substitution mechanisms. *American Mineralogist*, vol 90, pp 316-328.

MacDonald, M.A. (2001) Geology of the South Mountain Batholith, Southwestern Nova Scotia. *Nova Scotia Department of Natural Resources, Open File Report ME 2001-2*.

MacDonald, M.A., Horne, R.J., Corey, M.C., and Ham, L.J. (1992). An overview of recent bedrock mapping and follow-up petrological studies of the South Mountain Batholith, southwestern Nova Scotia, Canada. *Atlantic Geology*, vol 28, pp 7-28.

Macdonald, R., Rogers, N.W., Bagiński, B., and Dzierżanowski, P. (2010). Distribution of gallium between phenocrysts and melt in peralkaline salic volcanic rocks, Kenya Rift Valley. *Mineralogical Magazine*, vol 74(2), pp. 351-363.

Maciag, B.J., Brenan, J.M. and Hanley, J.J. (2021) Development of new mineralization pathfinders for the South Mountain Batholith (NS) using biotite and apatite trace element geochemistry. Final Report submitted to the Mineral Deposits Research Fund, March, 2021.

Manning, D.A.C. (1981). The Effect of Fluorine on Liquidus Phase Relationships in the System Qz-Ab-Or with Excess Water at 1 kb. *Contributions to Mineralogy and Petrology*, vol 76, pp 206-215.

Mohammadi, N., Lentz, D.R., Mcfarlane, C.R.M., and Yang, X. (2021). Biotite composition as a tool for exploration: An example from Sn-W-Mo-bearing Mount Douglas Granite, New Brunswick, Canada. *Lithos*, vol 382-383. doi: 10.1016/j.lithos.2020.105926

Paton, C., Hellstrom, J., Paul, B., Woodhead, J. and Hergt, J. (2011) Iolite: Freeware for the visualisation and processing of mass spectrometric data. Journal of Analytical Atomic Spectrometry. doi:10.1039/c1ja10172b.

Petrus, J.A., Chew, D.M., Leybourne, M.I. and Kamber, B.S. (2017) A new approach to laser-ablation inductively-coupled-plasma mass-spectrometry (LA-ICP-MS) using the flexible map interrogation tool 'Monocle'. *Chemical Geology*, vol 463, pp 76-93.

Pichavant, M., Villaros, A., Deveaud, S., Scaillet, B., and Lahlafi, M. (2016). The influence of redox state on mica crystallization in leucogranitic and pegmatitic liquids. *The Canadian Mineralogist*, vol 54, pp 559-581.

Shellnut, J.G., and Dostal, J. (2012). An evaluation of crustal assimilation within the Late Devonian South Mountain Batholith, SW Nova Scotia. *Geological Magazine*, vol 149(3), pp 353-365. doi: 10.1017/S0016756811000665

Shellnut, J.G., and Dostal, J. (2015). Granodiorites of the South Mountain Batholith (Nova Scotia, Canada) derived by partial melting of Avalonia granulite rocks beneath the Meguma terrane: Implications for the heat source of the Late Devonian granites of the Northern Appalachians. *Tectonophysics*, vol 655, pp 206-212. doi: 10.1016/j.tecto.2015.06.001

Stashin, Sydney. (2017). Investigating possible hybridization of the Peggys Cove granite section of the Halifax Pluton, South Mountain Batholith, Nova Scotia (Unpublished BSc Honours thesis). Dalhousie University, Halifax, Nova Scotia.

Tate, M.C., and Clarke, D.B. 1997. Compositional diversity among Late Devonian peraluminous granitoid intrusions in the Meguma Zone of Nova Scotia, Canada. *Lithos*, vol 39, pp 179–194.

Appendix A: Petrographic Descriptions

Please see the attached supplementary file “Appendix A Petrographic Descriptions.pdf” for the full description the hand samples and thin sections used in this study.

Appendix B: Biotite Major and Spot Analysis Data

Please see the attached supplementary file “Appendix B SGP-NRP Biotite Data.xlsx” for the whole rock analysis data (sheet 1), biotite major element data (sheet 2), and biotite minor element spot analysis data (sheet 3) for all samples from this study.

Appendix C: Biotite Trace Element Maps

Please see the attached supplementary file “Appendix C Figures.pdf” for all the trace element maps produced during this study. Please also see the attached supplementary file “Appendix C Map Summary.xlsx” for summaries of all the zoning patterns for all the maps (sheet 1), and for the list of maximum concentration scales for each map (sheet 2), as the scale produced with these maps have a very fine print.

Appendix D: Regions of Interest Data

The following images are the regions of interest superimposed on the Ta trace element maps created for each sample. Data for all trace elements measured was extracted and can be found in the supplementary data files “SGP Map Measurements.xlsx” and “NRP Map Measurements.xlsx”.

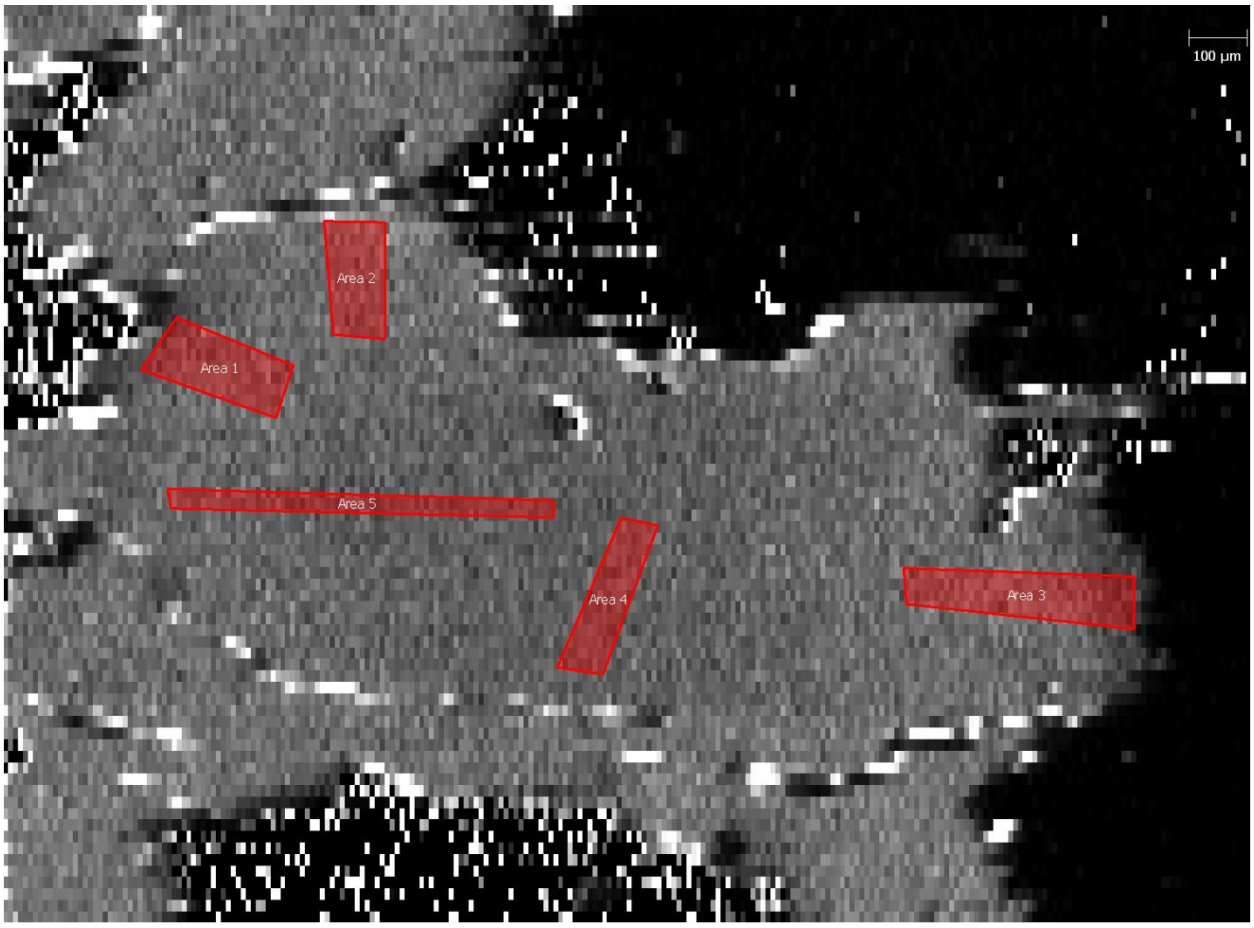

Regions of interest for sample 19BM-0004 Biotite 1.

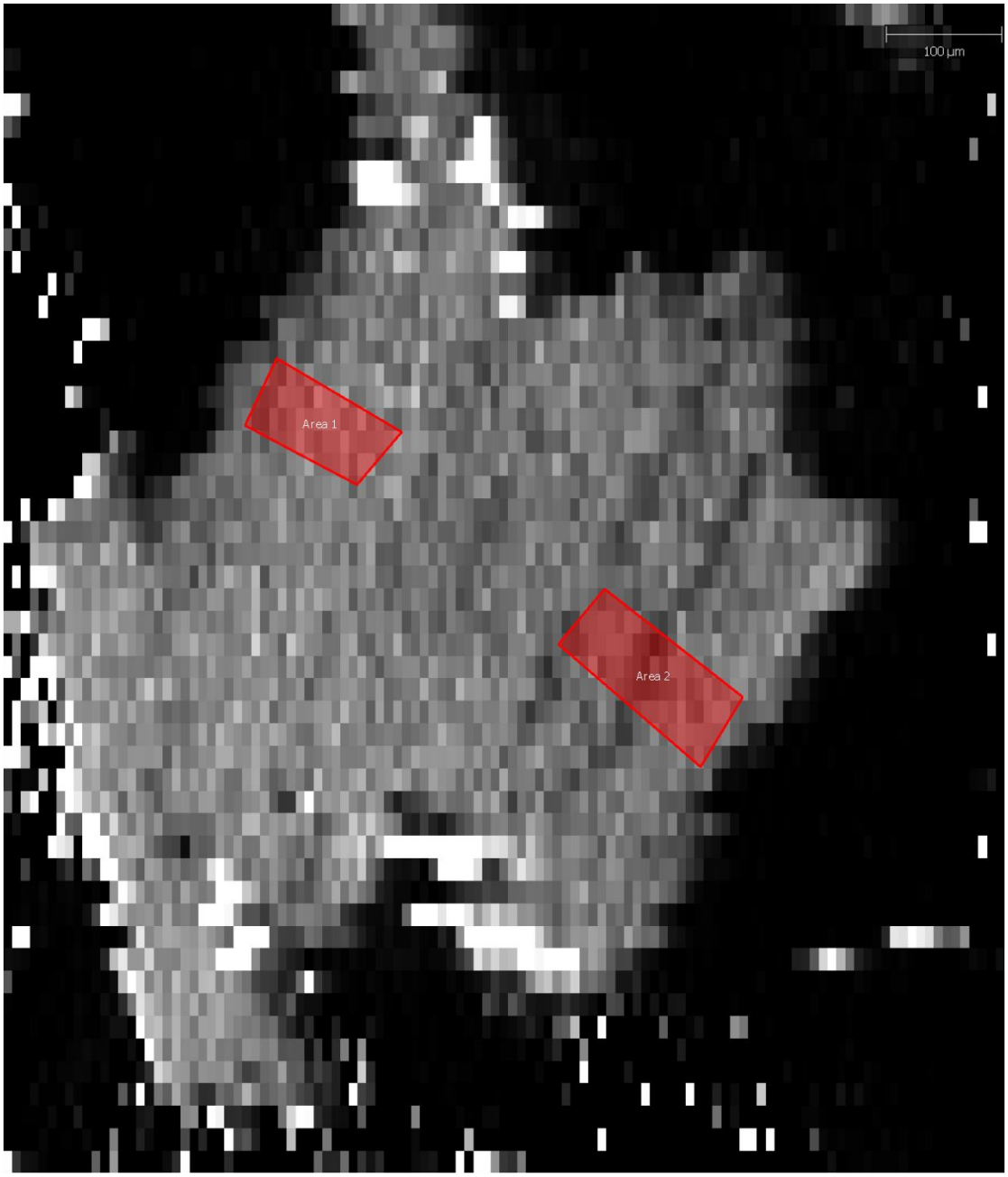

Regions of interest for sample 19BM-0004 Biotite 2.

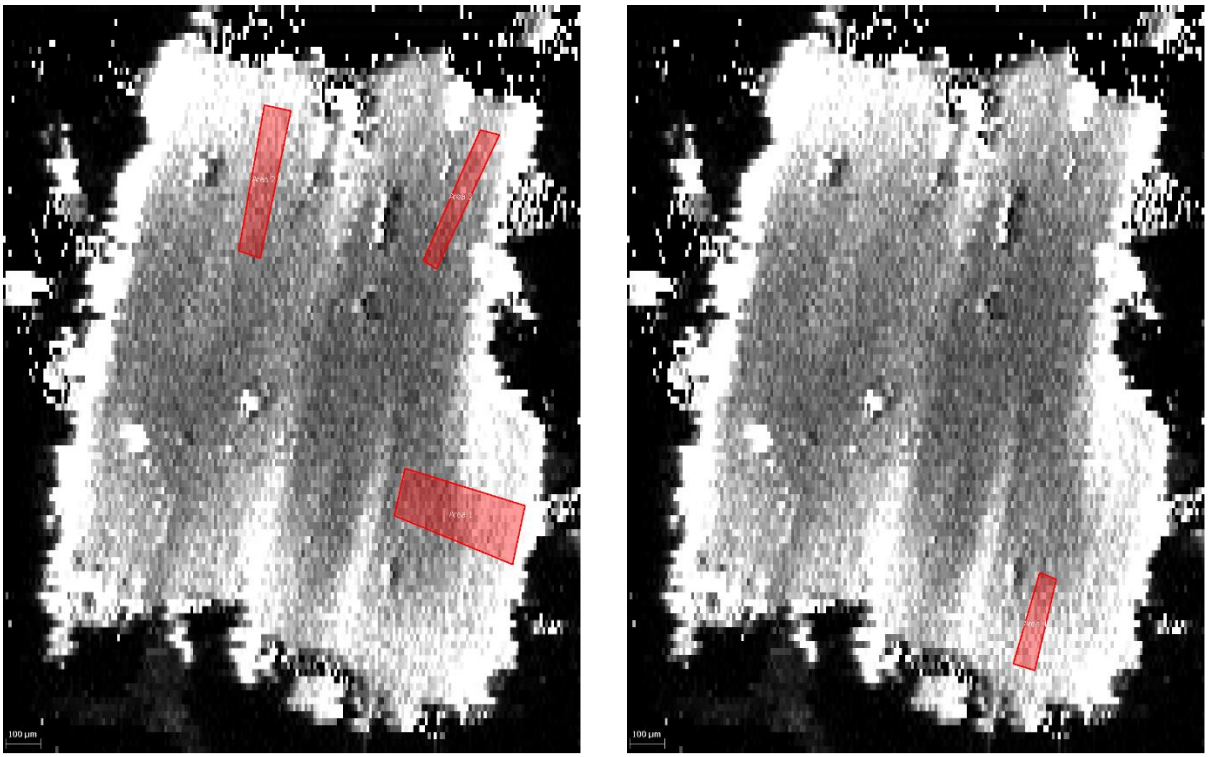

Regions of interest for sample A11-2268.

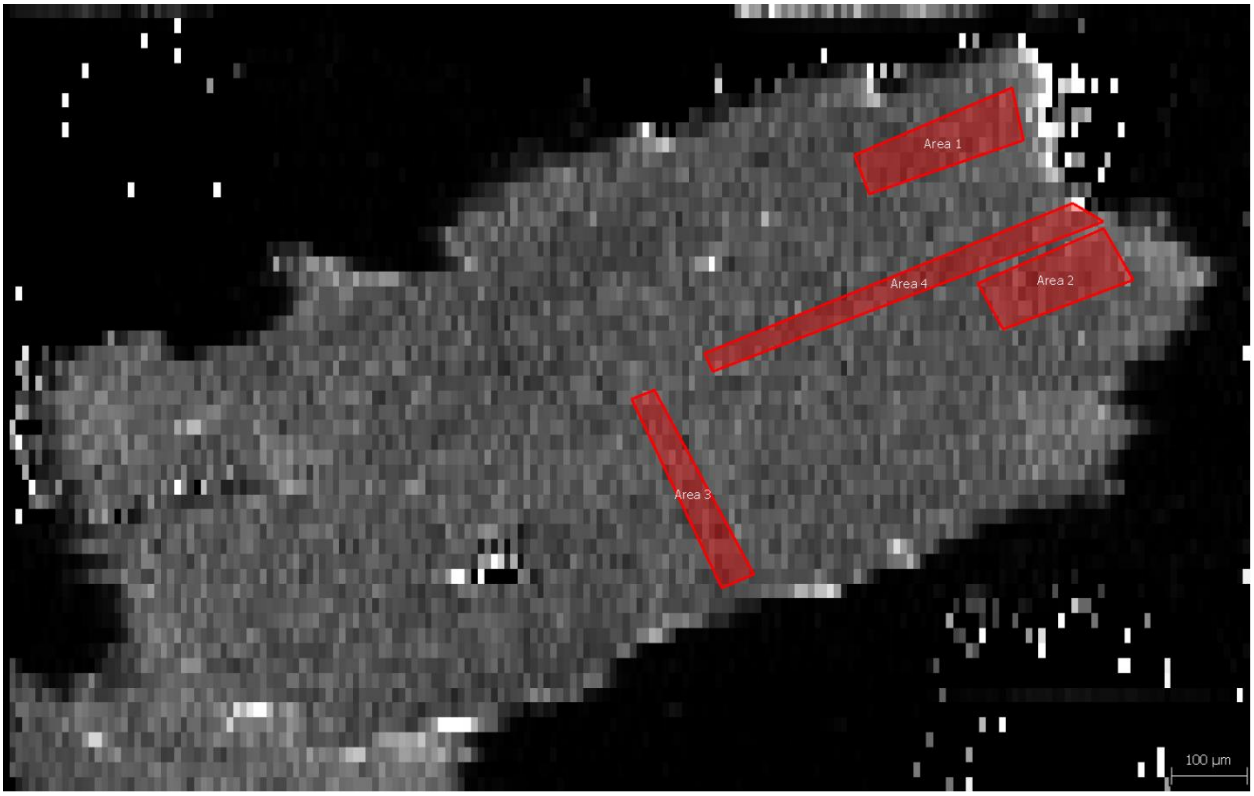

Regions of interest for sample A12-8007.

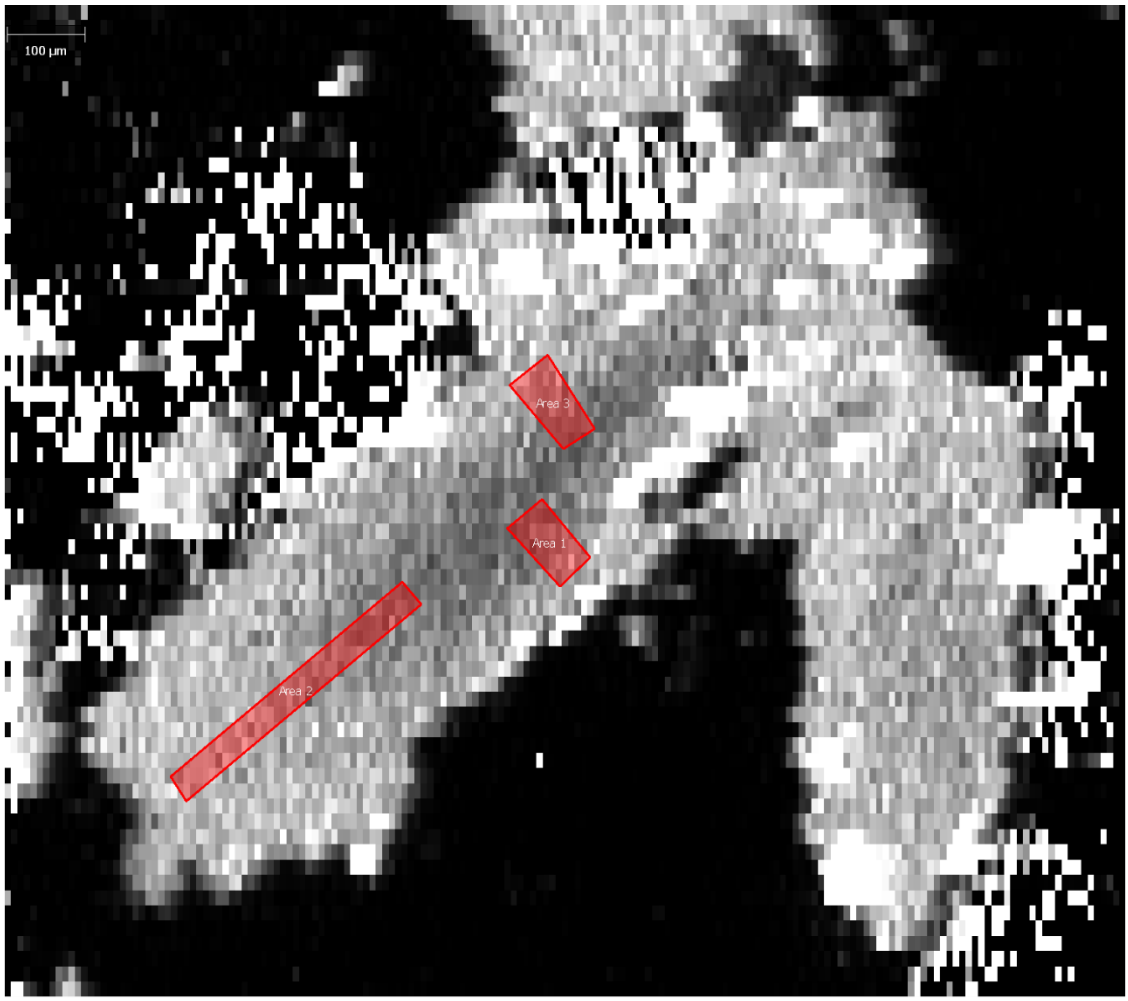

Regions of interest for sample A15-0102.

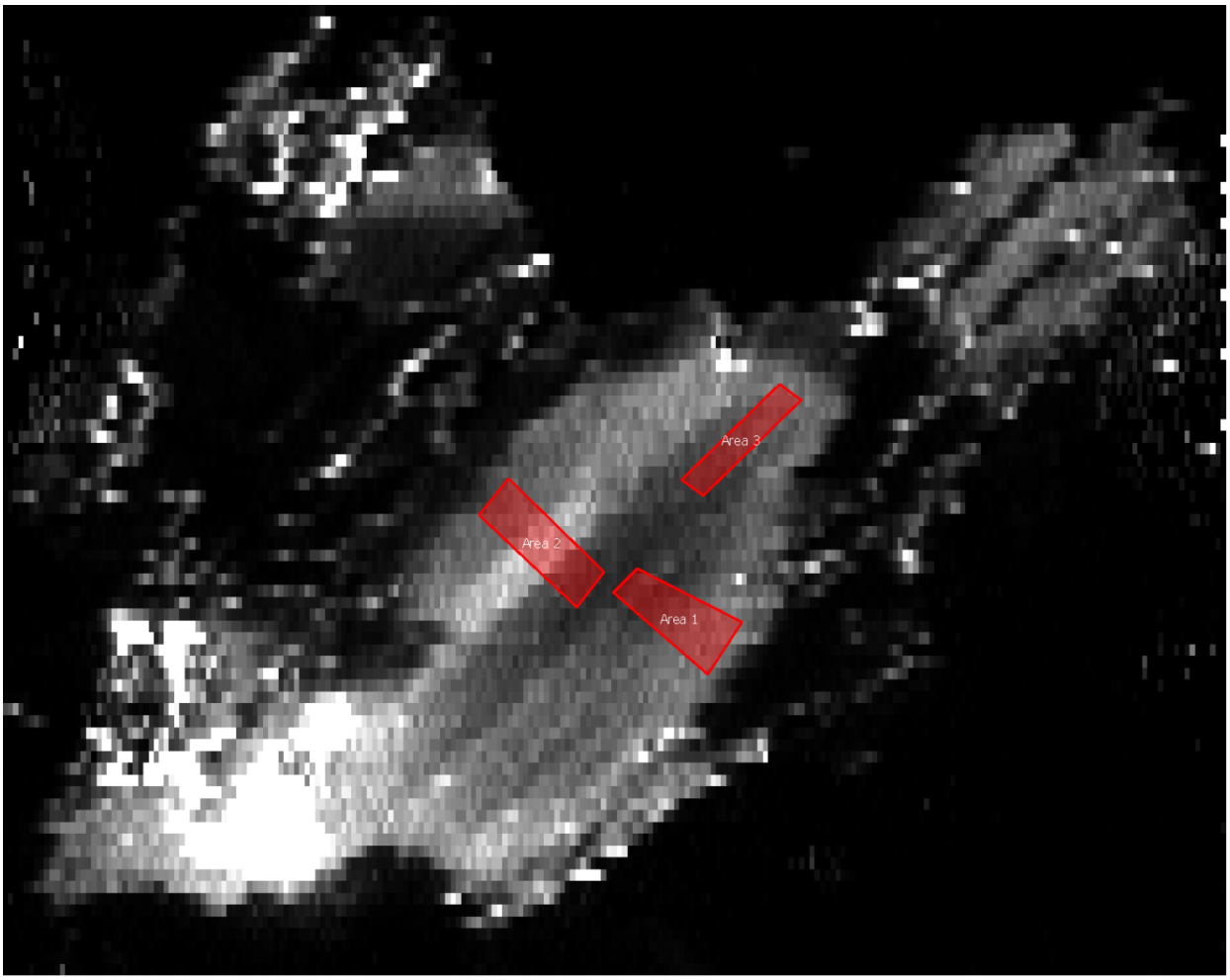

Regions of interest for sample A15-0114.

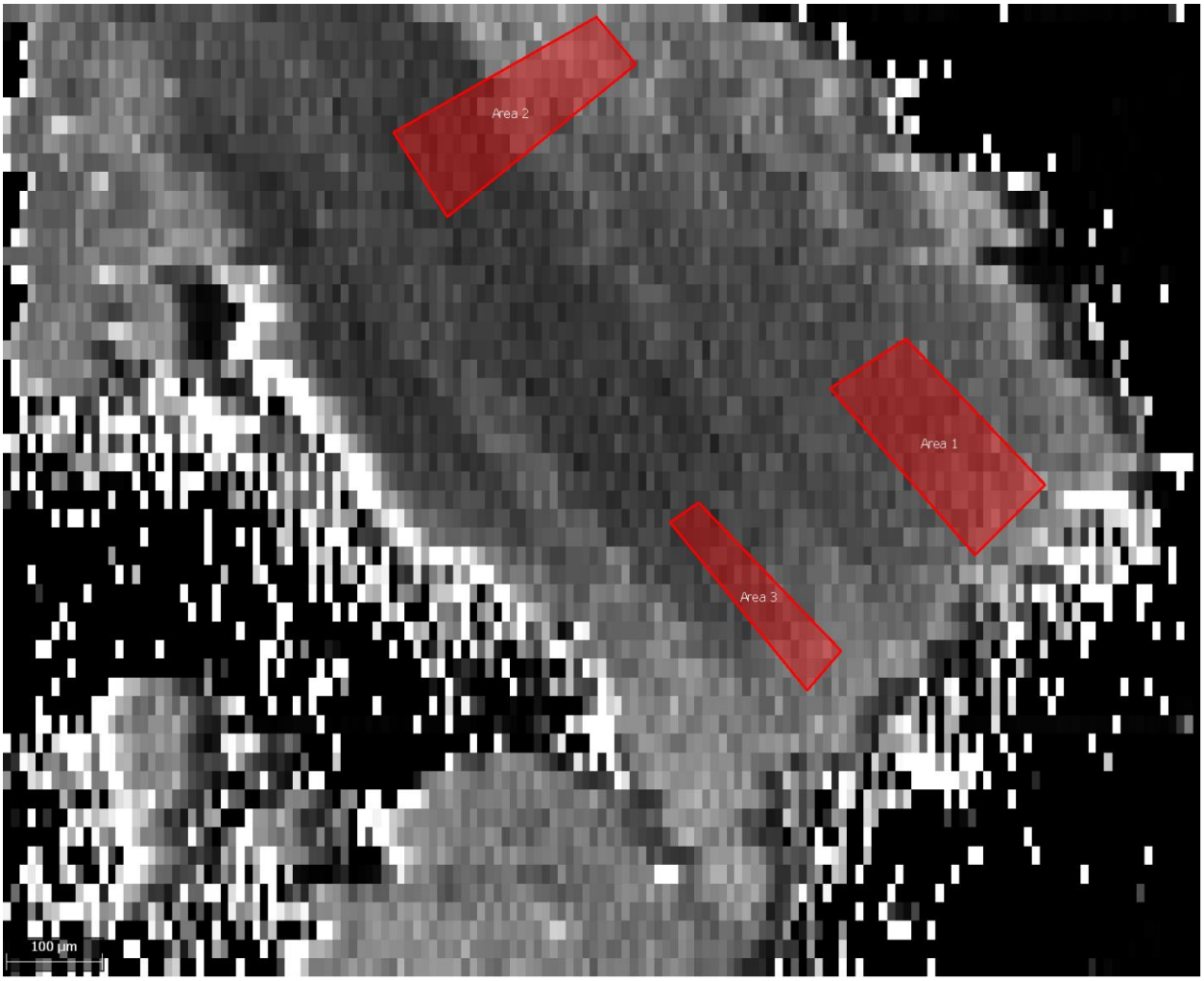

Regions of interest for sample A09-2378.

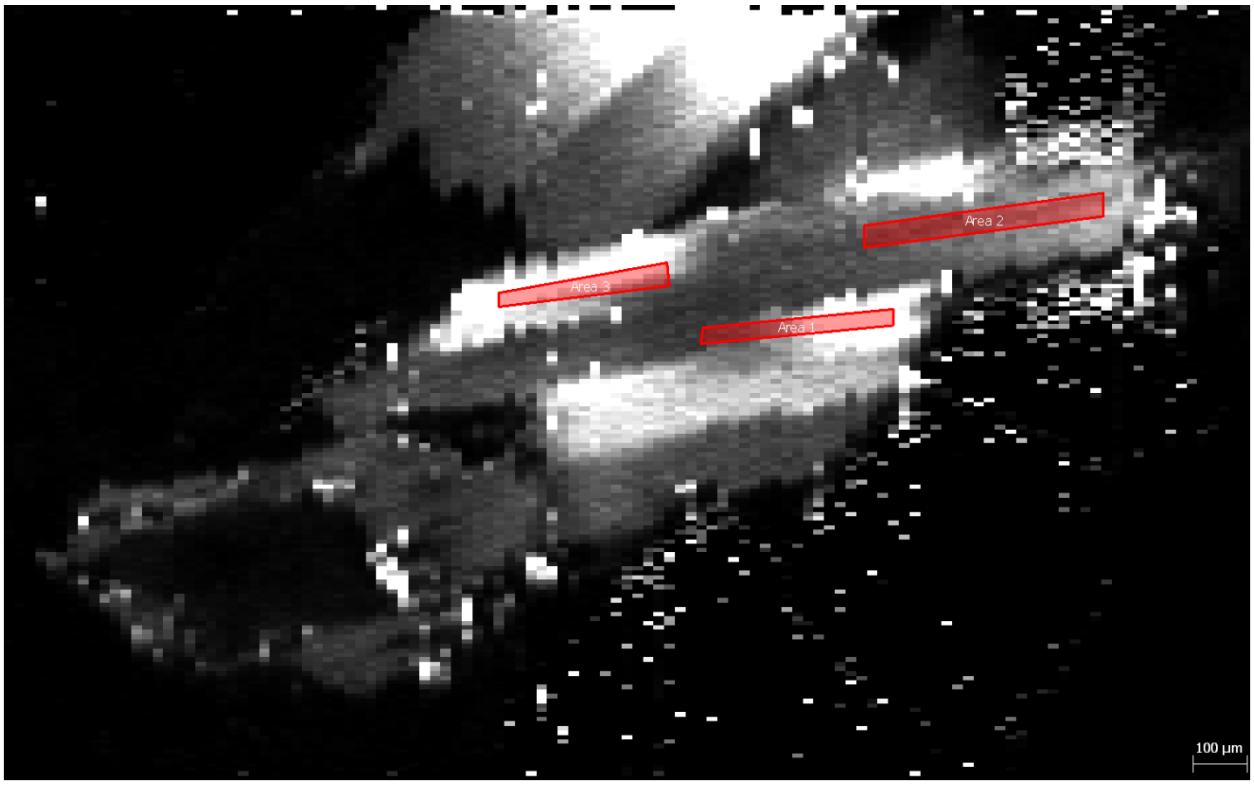

Regions of interest for sample A10-3020 C1 Biotite 2.

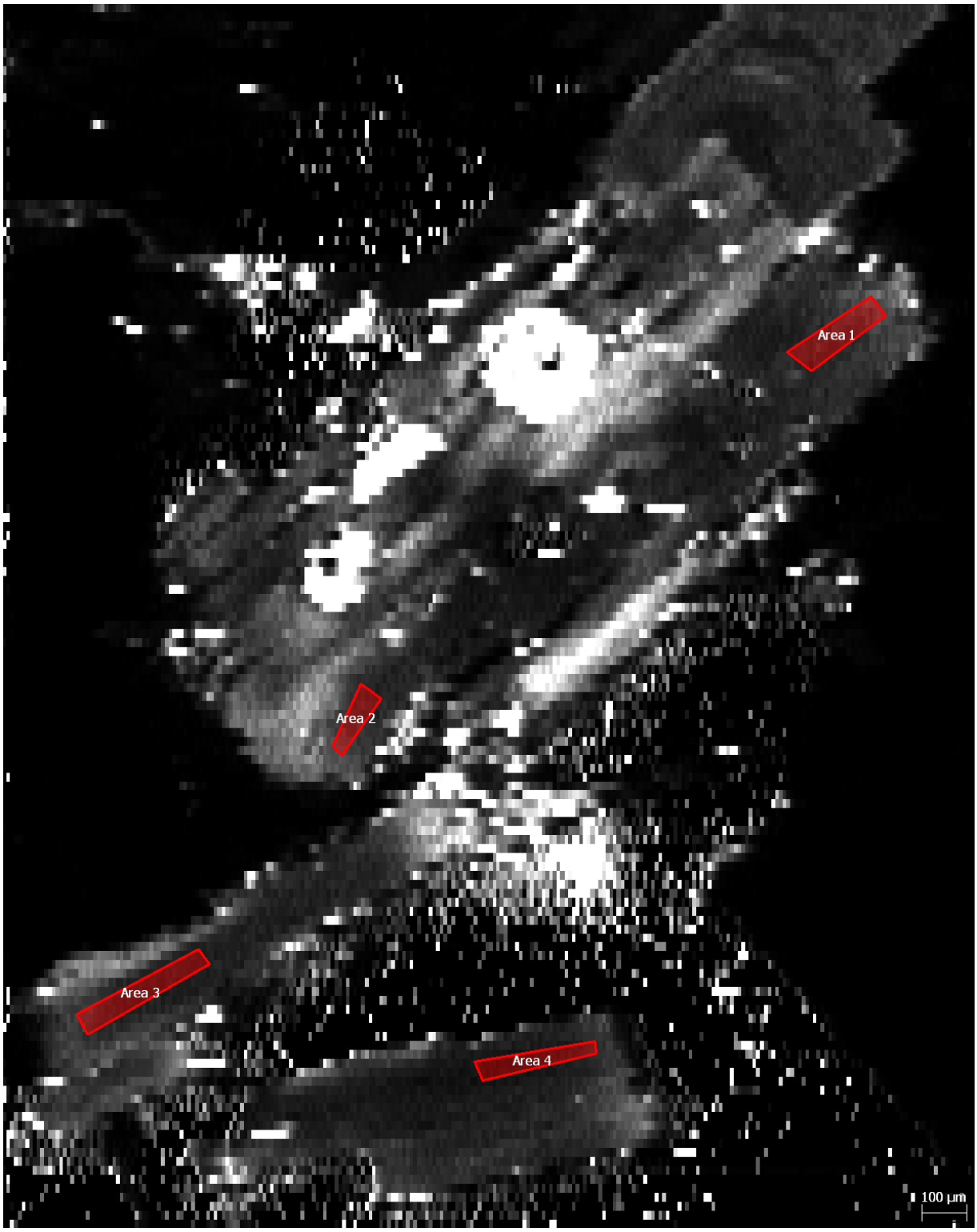

Regions of interest for sample A10-3020 C5 Biotite 1.

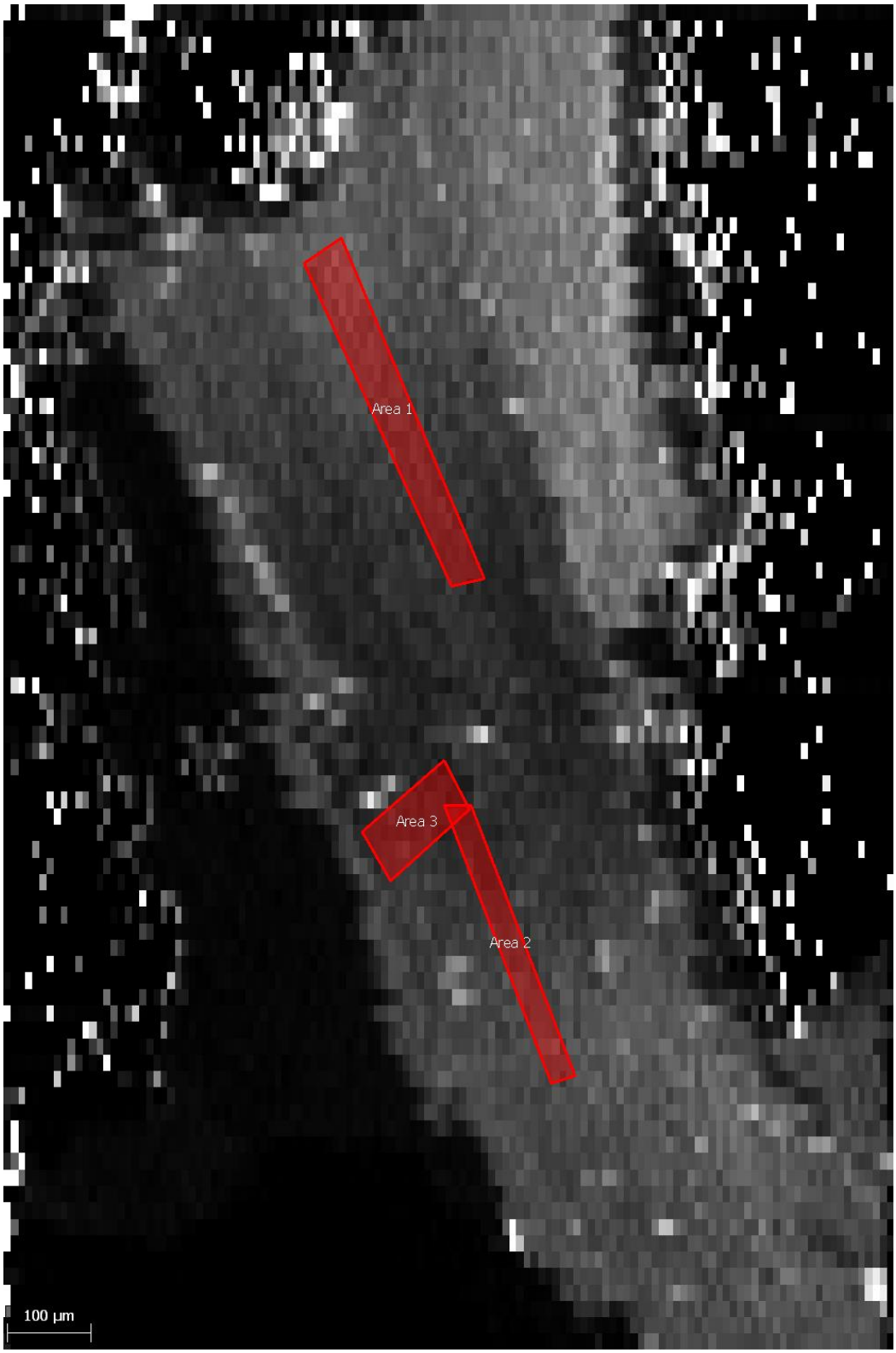

Regions of interest for sample A16-1171.